AGU PUBLICATIONS

Water Resources Research

RESEARCH ARTICLE
10.1002/2014WR016417

Applicability of bed load transport models for mixed-size sediments in steep streams considering macro-roughness

Johannes M. Schneider[1,2], Dieter Rickenmann[2], Jens M. Turowski[3], Kristin Bunte[4], and James W. Kirchner[1,2]

[1]Department of Environmental Systems Science, ETH Zurich, Zürich, Switzerland, [2]Mountain Hydrology and Mass Movements, Swiss Federal Research Institute WSL, Birmensdorf, Switzerland, [3]Helmholtz Centre Potsdam, GFZ German Research Centre for Geosciences, Potsdam, Germany, [4]Colorado State University, Engineering Research Center, Fort Collins, Colorado, USA

Key Points:
- Bed load Q_b at steep slopes S is typically overpredicted if macro-roughness R_L is neglected
- Critical- or boundary-shear-stress corrected for S or R_L improve Q_b prediction
- The shapes of fitted Q_b eqs. depend on whether critical- or boundary stress is corrected

Supporting Information:
- Supporting Information S1

Correspondence to:
J. M. Schneider,
johannes.martin.schneider@alumni.ethz.ch

Citation:
Schneider, J. M., D. Rickenmann, J. M. Turowski, K. Bunte, and J. W. Kirchner (2015), Applicability of bed load transport models for mixed-size sediments in steep streams considering macro-roughness, *Water Resour. Res.*, *51*, 5260–5283, doi:10.1002/2014WR016417.

Received 19 SEP 2014
Accepted 1 JUN 2015
Accepted article online 6 JUN 2015
Published online 14 JUL 2015

Abstract In steep mountain streams, macro-roughness elements typically increase both flow energy dissipation and the threshold of motion compared to lower-gradient channels, reducing the part of the flow energy available for bed load transport. Bed load transport models typically take account of these effects either by reducing the acting bed shear stress or by increasing the critical parameters for particle entrainment. Here we evaluate bed load transport models for mixed-size sediments and models based on a median grain size using a large field data set of fractional bed load transport rates. We derive reference shear stresses and bed load transport relations based on both the total boundary shear stress and a reduced (or "effective") shear stress that accounts for flow resistance due to macro-roughness. When reference shear stresses are derived from the total boundary shear stress, they are closely related to channel slope, but when they are derived from the effective shear stress, they are almost invariant with channel slope. The performance of bed load transport models is generally comparable when using the total shear stress and a channel slope-related reference shear stress, or when using the effective shear stress and a constant reference shear stress. However, dimensionless bed load transport relations are significantly steeper for the total stress approach, whereas they are similar to the commonly used fractional *Wilcock and Crowe* (WC) transport model for the effective stress approach. This similarity in the relations allows the WC model, developed for lower-gradient streams, to be used in combination with an effective shear stress approach, in steep mountain streams.

1. Introduction

1.1. Bed Load Transport in Steep Streams

Bed load transport can cause great damage in mountain regions and is a key process in landscape evolution. Accurately predicting bed load transport, however, is difficult due to the complex interactions between channel bed morphology and hydraulic conditions.

Bed load transport is driven by hydraulic forces, which in bed load transport equations are most commonly expressed by discharge, stream power, or shear stress. Shear stress is used throughout this study, but the presented concepts would be similar for discharge and stream power. In steady uniform flow, the dimensional shear stress τ and the dimensionless shear stress τ^* are related to the channel bed slope S (m/m) and flow depth or hydraulic radius r_h (m) according to

$$\tau = \rho g r_h S \tag{1a}$$

$$\tau^* = \frac{\tau}{(\rho_s - \rho) g D} \tag{1b}$$

where g is gravitational acceleration (m/s^2), ρ is water density (kg/m^3), ρ_s is sediment density (kg/m^3), and D is the diameter of a particle or grain-size fraction (m).

Bed load transport is not only influenced by the parameters specified in equations (1a and 1b) but also by form or macro-roughness, which is more important in mountain channels than in lower-gradient streams. Form roughness may be higher in steep streams due to (i) the channel form including pool-riffle to

plane-bed, step-pool, and cascade morphologies [*Montgomery and Buffington*, 1997]; (ii) an abundance of immobile boulders [e.g., *Nitsche et al*., 2011; *Yager et al*., 2007]; (iii) a variable channel width; and (iv) an increased number of bedrock constrictions and large woody debris [e.g., *Wohl*, 2000]. All these components contribute to what is commonly termed "form-roughness" or "macro-roughness," which significantly increases total flow resistance and reduces the fraction of the flow energy available for sediment transport [e.g., *Yager et al*., 2007; *Nitsche et al*., 2011; *Rickenmann and Recking*, 2011]. If these effects are not taken into account, predicted bed load transport rates overestimate observed bed load transport by orders of magnitude [e.g., *Bathurst et al*., 1987; *Chiari and Rickenmann*, 2011; *Lenzi et al*., 1999; *Recking et al*., 2012; *Rickenmann*, 2001, 2012; *Yager et al*., 2007, 2012a].

Bed load transport in steep streams is also affected by their greater structural bed stability and, therefore, erosion resistance [*Bunte et al*., 2013]. Possible explanations for the increased energy demand for sediment motion are given by *Lamb et al*. [2008] as "variable friction angles, grain emergence, flow aeration, changes to local flow velocity, and turbulent fluctuations," in addition to increased drag from large roughness elements. Two concepts exist for describing the critical conditions for initiation of particle motion in bed load transport calculations [*Bathurst*, 2013; *Wilcock*, 1988]: the flow competence method, in which the critical condition is defined by the maximum particle size moved at a given flow with a related "critical" shear stress [*Montgomery and Buffington*, 1997; *Shields*, 1936], and the reference transport method, in which the critical condition is defined by a "reference" shear stress τ_r^* which corresponds to an arbitrarily defined small bed load transport rate [*Parker et al*., 1982]. It has been shown that both concepts are closely related to each other; for example, *Wilcock et al*. [2009] demonstrated for the *Meyer-Peter and Mueller* [1948] equation that $\tau_c^* = 0.996\ \tau_r^*$.

An increase in critical shear stress with increasing channel slope has been shown for both the critical Shields stress [*Bettess*, 1984; *Bunte et al*., 2013; *Ferguson*, 2012; *Green et al*., 2014; *Lamb et al*., 2008; *Prancevic and Lamb*, 2015a; *Prancevic et al*., 2014; *Recking*, 2009; *Shvidchenko et al*., 2001] and the reference shear stress [*Green et al*., 2014; *Mueller et al*., 2005]. These bed-slope-dependent critical shear stress values have all been derived using the total boundary shear stress, which does not account for energy dissipation due to macroroughness elements. However, reference shear stress values derived from total boundary shear stress have been found to differ from those derived from a reduced effective shear stress; when using a reduced effective shear stress, typical values of the critical/reference shear stress for steep streams are in the range of those reported for lower-gradient streams [*Gaeuman et al*., 2009; *Yager et al*., 2012a].

The critical conditions for initial motion of individual particle-size classes control how fractional transport rates relate to each other and thus are a key control on long-term morphodynamic evolution of streambeds. In unisized beds, particle mobility is typically related to absolute particle size, and larger, heavier particles require higher shear stress to be mobilized than smaller, lighter particles [*Buffington and Montgomery*, 1997; *Shields*, 1936]. But in beds with mixed grain sizes, as are typical for steep mountain streams, particle mobility depends not only on the absolute grain size but also on the relative grain size. Smaller particles are hidden behind larger pieces of gravel, and are therefore protected from the flow while larger particles are more exposed to the flow [e.g., *Egiazaroff*, 1965; *Einstein*, 1950; *Parker*, 2008; *Parker and Klingeman*, 1982; *Parker et al*., 1982; *Wiberg and Smith*, 1987]. These effects are known as hiding and exposure, and they can modulate the relative mobility of different grain-size fractions. If hiding and exposure effects exactly cancel out the effects of particle mass, the probability of entrainment for each grain is independent of grain size at a given hydraulic stress, resulting in a condition termed "equal mobility." The degree of size-selective transport is typically described by a so-called hiding function, which relates the dimensionless fractional reference shear stress τ_{ri}^* to the dimensionless reference shear stress for the median grain size τ_{rD50}^* by the hiding exponent b (equation (2)).

$$\frac{\tau_{ri}^*}{\tau_{rD50}^*} = \left(\frac{D_i}{D_{50}}\right)^b \tag{2}$$

Estimated hiding functions reflect both the method used to describe the critical condition for sediment entrainment (i.e., the reference approach, the flow competence method, or visual observation of grain motion) [cf. *Buffington and Montgomery*, 1997] and different degrees of size-selectivity, ranging up to almost equal-mobility conditions [e.g., *Ashida and Michiue*, 1973; *Andrews et al*., 1987; *Bathurst*, 2013; *Green et al*.,

2014; *Mao et al*., 2008; *Parker* 1990; *Parker and Klingeman*, 1982; *Parker et al*., 1982; *Powell et al*., 2001; *Recking*, 2009; *Wilcock and Crowe*, 2003].

Finally, bed load transport in steep streams may also be affected by the sediment supply available for transport [e.g., *Bathurst*, 2007; *Recking*, 2012; *Yager et al*., 2012b]. Supply limitation often results in bed load overpredictions at steep slopes, if it is not considered adequately in a transport equation; however, in this study, we do not account for sediment supply issues.

1.2. Empirical Elements of Bed Load Transport Equations

Although most proposed bed load transport functions are based on physical consideration of the transport process, they also depend on empirical fits to data from flume studies or field observations. Important elements of this fitting procedure are illustrated in Figure 1, which presents synthetic bed load transport data sets for various streams in terms of the dimensionless transport rate W^* and the bed shear stress ratio τ^*/τ_r^* (equation (3)).

$$W^* = \frac{Rgq_{bVol}}{u^{*3}} \tag{3}$$

where $R = \rho_s/\rho_s - 1$, q_{bVol} is the volumetric bed load transport rate per unit width ($m^3\ s^{-1}\ m^{-1}$), and $u^* = (\tau/\rho)^{0.5}$ is the shear velocity.

Three main elements are important in the fitting procedure (see caption to Figure 1): (i) calculating the shear stress τ^* or the reduced (termed "effective") shear stress $\tau^{*\prime}$, (ii) determining the reference shear stress τ_r^*, and (iii) choosing the transport function including its prefactor.

1. When bed load transport equations are applied to different bed and flow characteristics than those from which they were derived from, a major challenge is calculating the flow energy available for bed load transport, i.e., an effective shear stress $\tau^{*\prime}$ (which controls the horizontal position of the data points in Figure 1). One of the earliest approaches to account for flow resistance due to form- or macro-roughness is to partition total flow resistance into grain and form resistance, as originally proposed by *Meyer-Peter and Mueller* [1948]. Similar approaches to partitioning between grain and form resistance, or between base level and macro-roughness, were later suggested by others [e.g., *Carson*, 1987; *Carson and Griffiths*, 1987; *Gomez and Church*, 1989; *Millar and Quick*, 1994; *Millar*, 1999; *Palt*, 2001; *Parker and Peterson*, 1980; *Rickenmann and Recking*, 2011; *Rickenmann et al*., 2006]. However, applications of a reduced effective shear stress $\tau^{*\prime}$ to bed load transport calculations, and comparisons with field data, remain limited [*Chiari and Rickenmann*, 2011; *Gaeuman et al*., 2009; *Nitsche et al*., 2011, 2012; *Wilcock*, 2001; *Wilcock et al*., 2009].

2. Another approach to collapsing the experimental data sets onto a single function (see caption to Figure 1) is based on adjusting the reference (or critical) shear stress. The choice of appropriate values for τ_r^* (or τ_c^*) affects the horizontal position of the experimental data sets in Figure 1, e.g., an increase in τ_r^* or τ_c^* shifts a data set to the left. In the case of fractional transport models that are based on a hiding function (equation (2)), the collapse of fractional transport rates is based on the fractional reference shear stress of each grain-size fraction (τ_{ri}^*); the derivation of τ_r^* and τ_{ri}^* goes back to *Parker et al*. [1982] and is described in more detail below in section 2.3.2.

3. The third important element refers to the choice of the transport function and its prefactor. In Figure 1, the selected transport function determines the steepness of the transport relation, while its prefactor controls the vertical position relative to the experimental data. For example, in the *Meyer-Peter and Mueller* [1948] transport equation, both *Hunziker and Jaeggi* [2002] and *Wong and Parker* [2006] suggested to reduce the prefactor from a value of 8 in the original equation to a value of about 5, based on a reanalysis of the experimental data. For a reference-shear-stress-based transport equation such as that of *Wilcock and Crowe* [2003], the dimensionless transport rate W^* increases as a power law function of the bed shear stress ratio τ^*/τ_r^*, with an exponent $m = 7.5$ for τ^*/τ_r^* ratios smaller than about 1.3.

To date, no systematic investigation, based on field data, has determined how reducing the boundary shear stress (point 1 above) or increasing the critical or reference shear stress (point 2 above) affects the shape of the transport relation (point 3 above) or the accuracy of its predictions. However, in one prior study [*Yager et al*., 2012a], reducing the boundary shear stress provided highest predictive accuracy for two specific mountain streams.

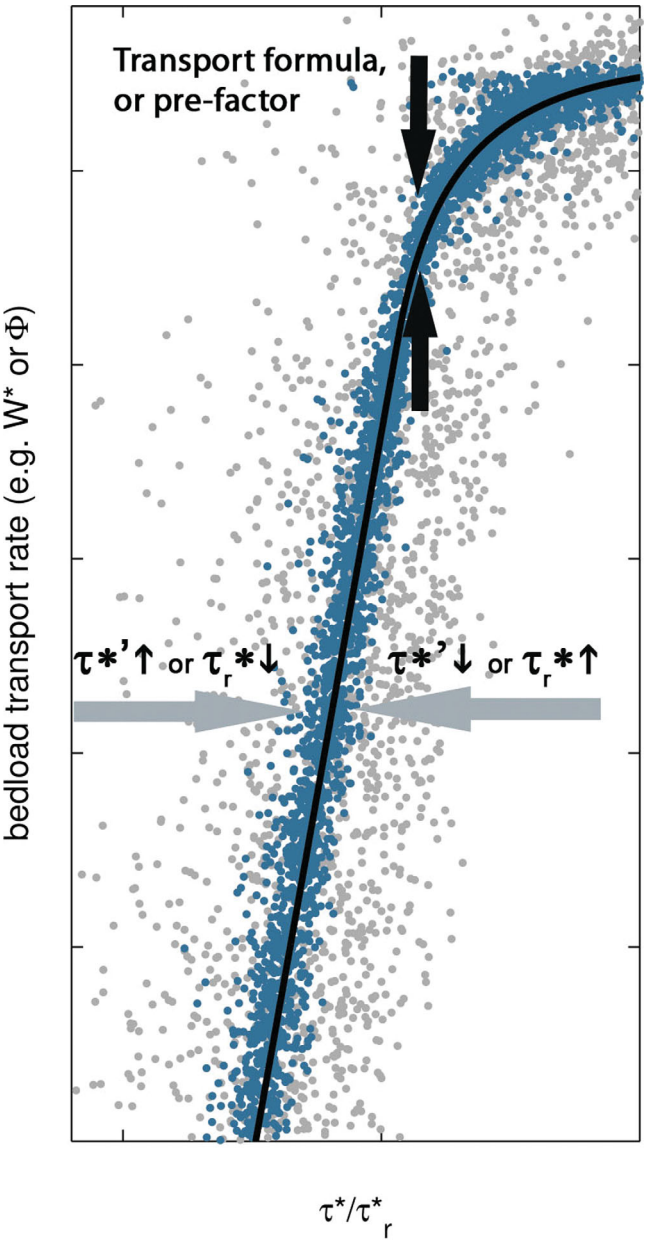

Figure 1. Illustration of a similarity collapse for bed load transport model development. Varying the effective shear stress $\tau^{*\prime}$ and/or the reference shear stress τ_r^* allows the scattered data points (gray dots) to be moved left or right. Ideally, it is possible to collapse the adjusted data points to represent a well-defined relation (blue dots). The mathematical bed load transport equation (black line) determines the rate of change of transport intensity with increasing shear stress, and the prefactor determines the vertical position in the diagram. Note: data points in this illustration are randomly generated. The shape of the example bed load relation corresponds to the *Wilcock and Crowe* [2003] equation.

In this study, we use high-quality field data sets of fractional bed load transport data covering a wide range of stream characteristics. Based on those field data sets, we analyze how using either total or effective shear stress affects the derived reference shear stress τ_r^* and thus the similarity collapse between the dimensionless transport rate W^* and the bed shear stress ratio τ^*/τ_r^*. We further examine how different adjustments of the bed load transport function, which are based either on fractional or total bed load transport data, affect bed load transport predictions. The overall goal is to demonstrate how the dimensionless reference shear stress (τ_r^*), the hiding exponent (b), and the exponents of the fractional and total transport equations (m) vary across wide ranges of bed gradients, and how they depend on the way that τ^* is determined. Our analysis showed few clear relationships of τ_r^*, b, and m to other characteristics of the field sites, so these are presented in the supporting information.

2. Field Data and Analysis

The field sites used to investigate bed load transport cover a wide range of channel slopes, flow discharge rates, and grain sizes (Table 1). Channel slopes range from about 0.05% to 11%, bankfull flows range from 0.3 to 114 $m^3\ s^{-1}$, and the median grain size of the surface D_{50surf} ranges from 0.004 to 0.2 m. The selected streams are compiled from the bed load trap data provided by *Bunte et al*. [2004, 2008, 2014, hereinafter Bunte] including 10 U.S. streams in Colorado, Wyoming, and Oregon, as well as the data from Oak Creek, Oregon, USA [*Milhous*, 1973], and data from two Swiss streams, Erlenbach (denoted *EB*) and Riedbach (denoted *RB*). To extend the range of bed gradients and grain sizes, the data set was complemented by data from *King et al*. [2004, hereinafter King] and *Williams and Rosgen* [1989, hereinafter WR]. The King data set has been analyzed in detail in many previous publications [e.g., *Barry*, 2004; *Barry et al*., 2008; *Mueller et al*., 2005; *Muskatirovic*, 2008; *Recking*, 2010; *Whiting et al*., 1999].

2.1. Bed Load Transport Data and Measurement Techniques

Fractional bed load transport rates were determined for the Bunte data set and the Riedbach data [*Schmid*, 2011] using portable bed load traps. The bed load traps consist of an aluminum frame with an

Table 1. Stream Characteristics[a]

	Source	Stream[b]	State, Country	S (m/m)	A (km^2)	Q_{bkf} (m^3/s)	D_{30Surf} (m)	D_{50Surf} (m)	D_{84Surf} (m)	Meas. Tech.[c]	Number of Values
Main Data set		Erlenbach	Schwyz, CH	0.11	0.7	1.5	0.02	0.06	0.21	MBB	49
		Riedbach	Valais, CH	0.026	18	3.0	0.02	0.06	0.16	BLT	53
	Bunte	St. Louis Cr.	Colorado, USA	0.017	34.0	4.0	0.04	0.08	0.16	BLT	42
	Bunte	Cherry Cr.	Oregon, USA	0.025	41.0	3.1	0.01	0.05	0.14	BLT	21
	Bunte	Litl. Granite Cr. A	Wyo., USA	0.017	55.0	5.7	0.03	0.06	0.13	BLT	58
	Bunte	E. St. Louis Cr. A	Colorado, USA	0.093	8.0	0.7	0.05	0.11	0.26	BLT	93
	Bunte	E. St. Louis Cr. B	Colorado, USA	0.093	8.0	0.7	0.05	0.11	0.26	BLT	133
	Bunte	Halfmoon Cr.	Colorado, USA	0.014	61.0	6.2	0.03	0.05	0.19	BLT	176
	Bunte	Hayden Cr.	Colorado, USA	0.039	40.0	1.9	0.04	0.06	0.16	BLT	192
	Bunte	E. Dallas Cr.	Colorado, USA	0.017	34.0	3.7	0.03	0.06	0.12	BLT	169
	Bunte	Fool Cr.	Colorado, USA	0.044	3.0	0.3	0.02	0.05	0.12	BLT	172
	Bunte	NF Swan Cr.	Colorado, USA	0.03	16.0	1.3	0.02	0.04	0.12	BLT	212
	Bunte	Litl. Granite Cr. B	Wyo., USA	0.012	13.0	2.8	0.04	0.07	0.14	BLT	62
	Milhous [1973]	Oak Cr.	Oregon, USA	0.0014	6.7		0.03	0.05	0.10	Vort.	43
HS Data set	*King et al.* [2004]	Big W. R. nr. Ket.	Idaho, USA	0.009	356	22	0.05	0.12	0.25	HS	100
		Boise R.	Idaho, USA	0.004	2,153	167	0.03	0.07	0.14	HS	82
		Dollar Cr.	Idaho, USA	0.015	42	6.4	0.04	0.07	0.15	HS	85
		Lochsa R.	Idaho, USA	0.004	3,054	446	0.09	0.15	0.25	HS	72
		MF Red R.	Idaho, USA	0.002	128	9.3	0.05	0.07	0.09	HS	200
		MF Salmon R.	Idaho, USA	0.006	2,693	214[a]	0.09	0.14	0.29	HS	64
		NFCl. Water R.	Idaho, USA	0.004	3,352	453	0.03	0.06	0.27	HS	72
		Rapid R.	Idaho, USA	0.0005	279	17.7	0.05	0.09	0.17	HS	190
		Salmon R. bl. Ynk. F	Idaho, USA	0.011	2,100	118[a]	0.07	0.10	0.28	HS	60
		Salmon R. nr. Obs.	Idaho, USA	0.003	243	12.6[a]	0.04	0.06	0.13	HS	50
		Salmon R. nr. Shp.	Idaho, USA	0.007	16,153	326[a]	0.05	0.10	0.17	HS	61
		Selway R.	Idaho, USA	0.002	4,955	651	0.12	0.20	0.27	HS	72
		SF Payette R.	Idaho, USA	0.002	1,164	86	0.03	0.06	0.15	HS	72
		Squaw Cr. USGS	Idaho, USA	0.004	185	5.1	0.03	0.04	0.07	HS	92
		Thompson Cr.	Idaho, USA	0.01	56	2.5	0.04	0.07	0.11	HS	84
	Williams and Rosgen [1989]	Susitna R. nr. Talk.	Alaska, USA	0.0153	16,369		0.02	0.05	0.10	HS	39
		Talkeetna R. nr. Talk.	Alaska, USA	0.004	5,195	114	0.03	0.04	0.07	HS	42
		Buffalo Cr.	Colorado, USA	0.01			0.002	0.004	0.01	HS	20
		Horse Cr.	Colorado, USA	0.001			0.01	0.04	0.10	HS	21
		Lo. SF Williams F.	Colorado, USA	0.03	69	4.2	0.03	0.07	0.22	HS	16
		Williams F.	Colorado, USA	0.007	69	4.2	0.05	0.08	0.17	HS	15

[a] S: Channel slope; A: Basin area; and Q_{bkf}: bank full flow or return period of 1.5 years, respectively.
[b] Original stream descriptions occasionally abbreviated (Cr. = Creek; E = East; N = North; F = Fork; W = Wood; M = Main/Middle; L = Left; Lo = Lower; bl. = below; nr. = near; R. = River; S = South).
[c] *MBB*: Moving bed load basket system [*Rickenmann et al.*, 2012]; BLT: Bed load trap [*Bunte et al.*, 2004]; HS: *Helley and Smith* [1971] sampler with a 76 mm opening; *Vort.*: Vortex tube [*Klingeman*, 1979; *Milhous*, 1973].

opening of 300 mm × 200 mm and a downstream attached nylon mesh bag, with a mesh width of 4 mm (and 6 mm in the Riedbach; we discuss how we treat different minimum measured grain sizes at the end of section 2.2) [*Bunte et al.*, 2004, 2007]. The Oak Creek (Oregon, USA) fractional bed load transport measurements were taken using a vortex sediment sampler [*Milhous*, 1973; *Parker*, 1990; *Parker et al.*, 1982]. At the Erlenbach, an automatic moving bed load basket (*MBB*) system with a mesh size of 10 mm provides fractional bed load transport rates [*Rickenmann et al.*, 2012]. The *Williams and Rosgen* [1989] and *King et al.* [2004] data were collected with *Helley and Smith* [1971; hereinafter HS] pressure difference samplers [see also *Emmett*, 1980]. For more details on the bed load measurement techniques, see supporting information Text S1.

To base our study only on well-defined field-measured transport relations, we included from the WR and King data sets only those streams that yielded a coefficient of determination $r^2 > 0.5$ for fitted bed load transport relations in the form of (equation (4)):

$$Q_b = \alpha Q^{\beta} \tag{4}$$

Here Q_b is the total bed load transport rate (kg s^{-1}), Q is the flow discharge (m^3 s^{-1}), and α and β are empirical constants. We fitted equation (4) to all data available from each stream site using linear least squares regression on log-transformed values; r^2 was also determined on the log-transformed values.

In general, the HS samples have larger sampling uncertainties compared to other measurement techniques described in this study. One reason is the small 76.2 × 76.2 mm^2 opening compared to the 300 × 200 mm^2 opening of the bed load traps; another reason is the shorter sampling time (typically around 20–180 s) (for more details, see *Bunte et al*. [2005, 2008]). Therefore, we decided to analyze the HS samples separately from the data derived from the other measurement techniques. In the following, the data by Bunte, the Riedbach, Erlenbach, and Oak Creek data are denoted as the Main Data set, while the HS samples, including the WR and King data sets, are denoted as the HS Data set.

2.2. Streambed and Bed Load Grain-Size Distributions

Streambed surface grain-size distributions (GSDs) were determined using the *Wolman* [1954] pebble count method or a slightly modified version of it [*Bunte and Abt*, 2001a, 2000b; *Bunte et al*., 2009]. Subsurface samples were taken volumetrically and analyzed by sieve analysis. For more details on the GSD sampling techniques, see supporting information Text S2.

Bed material grain-size distributions of all streams, which were originally reported in various scales, were converted to the full phi scale (2, 4, . . . 1064 mm) for simplified computing and analysis. We ignored grain sizes less than 2 mm, because for many of the streams, smaller grain sizes had not been counted in the field according to the pebble count method. The pebble count method was applied to all study streams, except the WR streams, where the method applied was not fully reported. For the King and WR data set, the D_{50Surf} and D_{84Surf} grain sizes were derived from the converted phi-scale GSDs, not the original GSDs provided in the literature. Hence, the characteristic grain sizes used in this study occasionally deviate slightly from the values reported in other studies.

The bed load GSDs were converted to the same full phi scale as the bed surface and subsurface GSDs. The smallest sampled bed load grain sizes vary among data sets depending on the measurement technique, ranging from 0.0625 mm for the WR data set to 10 mm for the Erlenbach. We truncated the King and WR bed load GSDs at 2 mm, because for the following dimensionless analysis, we relate fractional transport rates to surface grain-size fractions, which are only quantified for size fractions larger than 2 mm. The variation in the minimum measured bed load grain size (2–10 mm) does not strongly affect the analysis relating fractional transport rates to the reference shear stress and acting bed shear stress, for two reasons: (1) the reference shear stress τ^*_{rD50} derived from the reference approach (see section 2.3.2) does not depend on the minimum considered bed load grain size. Rather, it depends on the D_{50Surf}, which again is related to the streambed surface GSD valid for $D > 2$ mm. (2) We did not find systematic trends by which the bed load transport relation exponents differ among grain-size fractions (see section 3.3.1), hence the outcomes of the analyses are not affected by the number or the coarseness of grain-size fractions involved. For the analysis of total transport rates, we define total bed load transport (also often termed bulk bed load transport in the literature) as all grains larger than 4 mm. This corresponds to the minimum grain size measured by the bed load traps. The resulting uncertainties/biases in total transport rates for the Riedbach ($D > 6$ mm) and the Erlenbach ($D > 10$ mm) are neglected.

2.3. Flow Hydraulics

Bed load transport is described throughout this study as a function of dimensionless shear stress τ^*, which is proportional to flow depth (or hydraulic radius) and channel slope (equation (1)). However, flow depth is often unmeasured in stream studies or may have large sampling uncertainties, and *Recking* [2010] argued that the predictive quality of bed load equations is improved when discharge is used instead of flow depth. Hence, instead of flow depths obtained from field measurements, we used hydraulic radii (r_h) that were back calculated from the measured flow discharge and average cross-sectional profiles of our study streams. We iteratively computed flow depth and width, hydraulic radius and cross-sectional area for each measured discharge, and reach-averaged velocity, using the variable power equation (VPE) of *Ferguson* [2007]:

$$u/u^* = \frac{a_1 a_2 (r_h/D_{84Surf})}{\sqrt{a_1^2 + a_2^2 (r_h/D_{84Surf})^{5/3}}} \tag{5}$$

where u is flow velocity (m s^{-1}), u^* is shear velocity $u^* = (g r_h S)^{0.5}$, r_h/D_{84} is the relative flow depth, and $a_1 = 6.5$ and $a_2 = 2.5$ are empirical constants. *Rickenmann and Recking* [2011] evaluated several flow

resistance equations based on a large field data set of flow velocity measurements in gravel-bed rivers and found that the VPE of *Ferguson* [2007] with $a_1 = 6.5$ and $a_2 = 2.5$ generally provided the best performance [cf. *Nitsche et al*., 2011], so we used those values in equation (5). Equation (5) implicitly accounts for large roughness elements and was found to also give good predictions of total flow resistance for flow conditions with small relative flow depths (r_h/D_{84}) in steep streams. The iterative calculation of the hydraulic parameters using equation (5) was performed on average cross sections derived from surveyed cross sections upstream of the sampling location for the Riedbach, the Erlenbach, and the *King et al*. [2004] data sets. For the U.S. bed load trap study, cross sections surveyed at or near the bed load trap location were used for computing the hydraulic parameters. For the *Williams and Rosgen* [1989] data set, a rectangular cross section was estimated from the given stream width.

2.3.1. Determination of Effective Shear Stress τ'

Two approaches are used in this study to estimate the increased flow resistance in steep streams due to macro-roughness elements (boulders, bedrock, and woody debris). The first approach [*Rickenmann and Recking*, 2011, hereinafter RR2011] is based on computing shear stress using a reduced energy slope S_{red} (equation (6)) instead of the actual channel slope [*Chiari and Rickenmann*, 2011; *Chiari et al*., 2010; *Nitsche et al*., 2011; *Rickenmann and Recking*, 2011; *Rickenmann*, 2012]. The concept of a reduced energy slope is based on flow-resistance partitioning between a base level flow resistance (f_o) and the total resistance (f_{tot}), which includes additional resistance due to large roughness elements at relatively small flows. The base level resistance (f_o) is calculated by extrapolating the Manning-Strickler relation to small relative flow depths, using a mean resistance coefficient $a_1 = 6.5$ as proposed by *Ferguson* [2007] and *Rickenmann and Recking* [2011]. Total resistance (f_{tot}) is determined with equation (5) above. The reduction of the energy slope also depends on the relative flow depth r_h/D_{84}, for more details see *Rickenmann and Recking* [2011] and *Rickenmann* [2012]:

$$S_{red} = S\left(\sqrt{\frac{f_0}{f_{tot}}}\right)^e \tag{6a}$$

$$\tau' = \rho g r_h S_{red} \tag{6b}$$

This approach is similar to flow resistance partitioning between grain and form resistance, as proposed in earlier studies [*Millar and Quick*, 1994; *Millar*, 1999]. We used an exponent of $e = 1.5$, which has been shown to substantially improve bed load transport estimates [*Meyer-Peter and Mueller*, 1948; *Nitsche et al*., 2011].

We also used the approach of *Wilcock et al*. [2009, hereinafter WC2009] to account for form resistance or macro-roughness, which generally corresponds to the approach earlier suggested in *Wilcock* [2001]. The *Wilcock et al*. [2009] equation determines grain resistance using a Manning-Strickler relationship and defines the reduced (effective) shear stress τ' via the D_{65} of the streambed surface (in mm):

$$\tau' = 17(SD_{65})^{0.25}u^{1.5} \tag{7}$$

Shear stress values τ' from equation (7) are very similar to those obtained using equation (6). For the sake of a simplified presentation, the results based on equation (7) are presented only in the supporting information. Both equations (6b) and (7) refer to dimensional forms of the shear stress and can be nondimensionalized using equation (1b).

2.3.2. Derivation of the Reference Shear Stress

The adjustment of the fractional dimensionless reference shear stress, used to collapse the fractional dimensionless transport rates (both within individual streams and between different streams), was determined following the reference approach of *Parker et al*. [1982] and *Wilcock and Crowe* [2003]. The dimensionless reference transport rate used in this study, denoted W_i^* for the ith size fraction, was set to 0.002. The fractional dimensionless transport rate W_i^* is defined by equation (8) as

$$W_i^* = \frac{Rgq_{biVol}}{F_i u^{*3}} \tag{8}$$

where F_i is the proportion of grain size i on the bed surface, q_{biVol} the volumetric fractional bed load transport rate per unit width ($m^3\ s^{-1}\ m^{-1}$), and $u^* = (\tau/\rho)^{0.5}$ is the shear velocity. In the following, if the

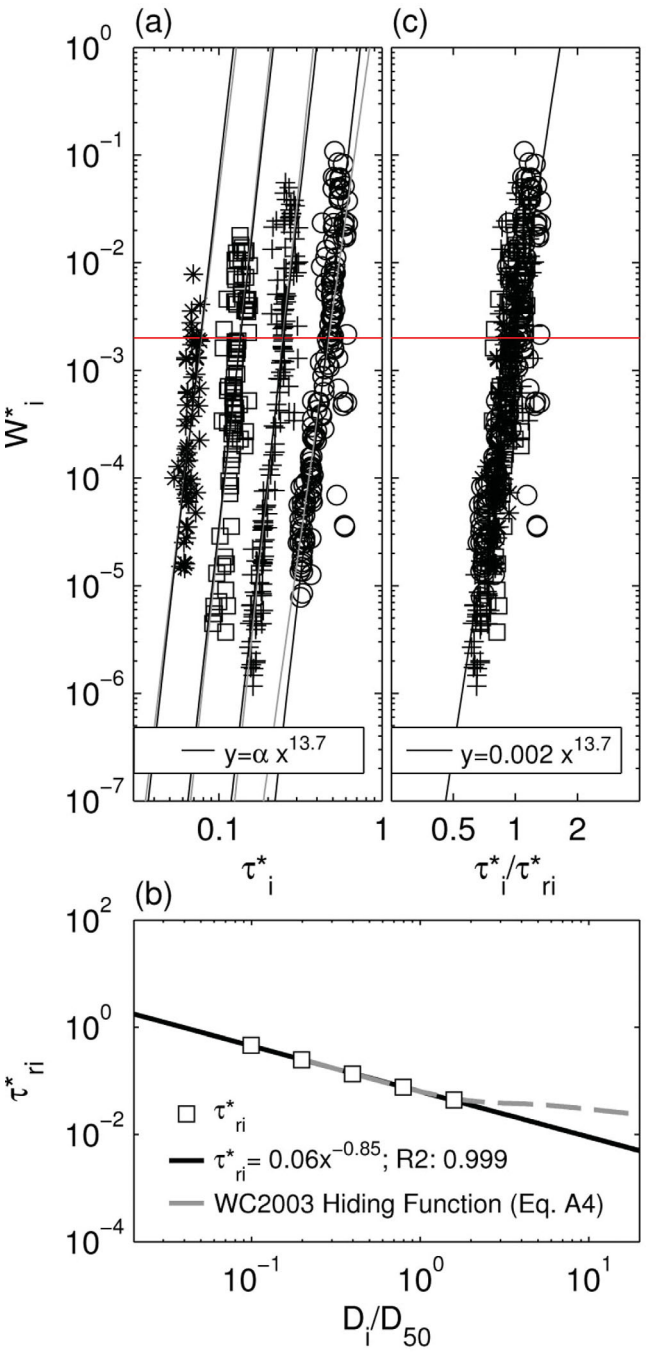

Figure 2. Reference approach [*Parker et al.*, 1982] applied to East Dallas Creek (Bunte Data set). (a) Power functions fitted to plots of fractional dimensionless bed load transport rates versus dimensional shear stress for 1 phi size classes from 4 mm (open circle) to 32 mm (asterisk), with free exponents m_i (gray lines) and a fixed averaged exponent $m_{i50} = 13.7$ (black lines). (b) Hiding function in the form of equation (2) with a constant exponent b (black line) and a variable exponent according to *Wilcock and Crowe* [2003] (gray dotted line, equation (A4)). (c) Collapse of fractional transport rates. Horizontal lines in Figures 2a and 2c represent the dimensionless transport rate $W^* = 0.002$.

dimensionless transport rate explicitly refers to an effective shear stress τ' (rather than a total shear stress), it is labeled as $W^{*\prime}$ (rather than W^*). The reference approach of *Parker et al.* [1982] includes the following four steps:

1. Fitting power functions ($W_i^* = a_i \tau_i^{*mi}$) to W_i^* and τ_i^* for each individual grain-size fraction i (shown for East Dallas Creek as an example in Figure 2a).
2. Fitting functions ($W_i^* = a_i \tau_i^{*mi50}$) for each grain-size fraction, with m_{i50} as the median of the exponents m_i derived in the previous step (Figure 2a).
3. Estimating τ_{ri}^* by selecting the value of τ_i^* corresponding to a reference transport rate of $W_i^* = 0.002$.
4. Fitting the relationship between τ_{ri}^* and D_{iSurf}/D_{50Surf}, thus determining the reference shear stress τ_{rD50}^* and the hiding exponent b (Figure 2b).

Based on the hiding function approach, it is possible to collapse fractional transport rates for a given channel reach onto a more-or-less single curve (Figure 2c). The resulting fractional transport power law relationship is defined in this study by the prefactor 0.002 and the median exponent m_{i50} (Figure 2c). Because the dimensionless reference shear stress τ_{ri}^* is a site-specific constant, the log-log slope of the relationship between W_i^* and τ_i^* is the same as the log-log slope of the relationship between W_i^* versus τ_i^*/τ_{ri}^*. Therefore, the exponents m_i (and m_{i50}, respectively) are the same in W_i^* versus τ_i^* relationships (e.g., Figure 2a) and W_i^* versus τ_i^*/τ_{ri}^* relationships (e.g., Figure 2c), and we use them interchangeably between these two contexts.

In addition to the dimensionless fractional reference shear stress, the reference shear stress $\tau_{rD50Surf}^*$ was also determined from total transport rates for $D > 4$ mm by fitting power functions to W_{tot}^* versus $\tau_{D50Surf}^*$ and identifying the intercept of the power law with $W_{tot}^* = 0.002$ [see also *Mueller et al.*, 2005]. The 4 mm criterion for W_{tot}^* was chosen because it is the minimum grain-size sampled with bed load traps, except at the Riedbach (6 mm) and the Erlenbach (10 mm). For those total transport computations, all HS samples were truncated at 4 mm as well.

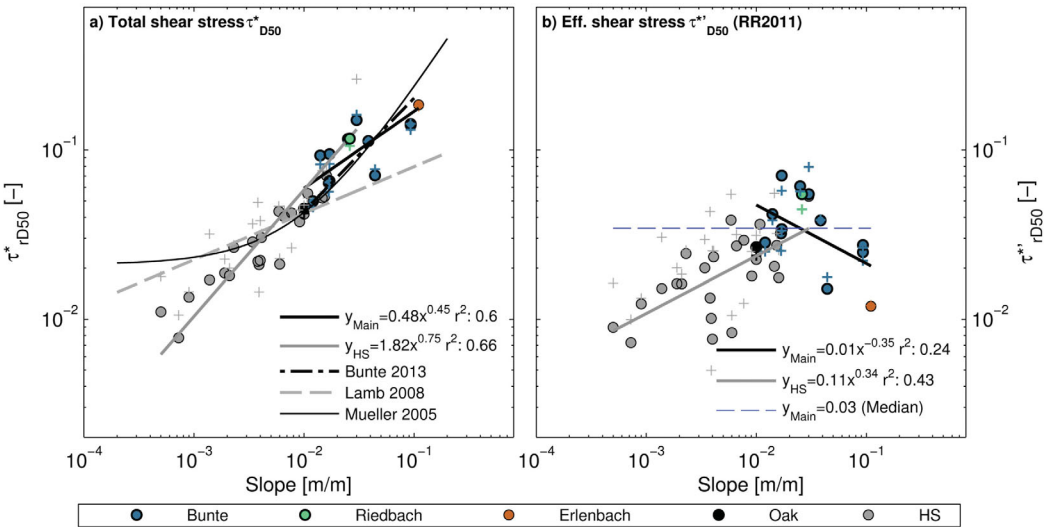

Figure 3. Dimensionless reference shear stress (τ^*_{rD50}) related to channel bed slope for (a) the *total* acting bed shear stress τ^*_{D50} and (b) the reduced *effective* shear stress $\tau^{*\prime}_{D50}$ (RR2011). Filled circles correspond to τ^*_{rD50} values from analyzing fractional transport rates (see reference approach section 2.3.2 and Figure 2b. Crosses indicate τ^*_{rD50} derived from analysis of total dimensionless transport rates. The thick black line was fitted to the Main Data set, and the thick gray line to the HS Data set, for τ^*_{rD50} derived from the analysis fractional transport rates. In Figure 3a, the empirical relations of *Bunte et al*. [2013], *Lamb et al*. [2008], and *Mueller et al*. [2005] are given. The dashed blue line in Figure 3b corresponds to the median τ^*_{rD50} from Main Data set.

3. Results

3.1. Reference Shear Stress (τ^*_{rD50})

3.1.1. τ^*_{rD50}—Derived From Fractional Bed Load Transport Rates

The dimensionless reference shear stress τ^*_{rD50} was derived from fractional transport rates based on the total boundary shear stress (Figure 3a and Table 2 and Table S1). The relationship between τ^*_{rD50} and channel slope for the Main Data set is defined by equation (9)

$$\tau^*_{rD50} = 0.48S^{0.45};\ \ r^2 = 0.63\ \ for\ \ S > 0.01 \tag{9}$$

and follows a similar pattern to that reported by *Mueller et al*. [2005] for the King data.

The relationship between τ^*_{rD50} and channel slope also resembles the critical shear stress relation of *Bunte et al*. [2013]. Note that *Bunte et al*.'s [2013] relation for the critical shear stress was derived from the same bed load transport data as used here, including the Oak Creek data; however, their calculation proceedure corresponds to the flow competence approach (cf. section 1). The τ^*_{rD50} values of the HS Data set generally exhibit similar trends with channel slope as τ^*_{rD50} values of the Main Data set (Figure 3a).

For the dimensionless reference shear stress $\tau^{*\prime}_{rD50}$ based on the (reduced) effective shear stress (equations (6) and (7)), the strong positive correlations of the reference shear stress $\tau^{*\prime}_{rD50}$ with channel slope S almost vanish (Figure 3b; see also Figure S3a for the WC2009 approach). The $\tau^{*\prime}_{rD50}$ relation with channel slope in the Main Data set (Figure 3b) is highly scattered with median values of about 0.03 (Table 3) and a slight negative trend. However, this negative trend is not supported by the independent HS data.

The computed τ^*_{rD50} for the total boundary shear stress (supporting information Figure S1) and the $\tau^{*\prime}_{rD50}$ for the reduced effective shear stress approaches (Figures S2 and S3) were also compared with several streambed characteristics. The streambed characteristics include the sand content [cf. *Wilcock and Crowe*, 2003], the degree of armoring D_{50Surf}/D_{50Sub} [cf. *Efthymiou*, 2012], the geometric standard deviation of the streambed surface grain-size distribution σ_{SG} [cf. *Gaeuman et al*., 2009], and the D_{84Surf}/D_{30Surf} ratio. The parameters representing the width of the GSD (D_{84Surf}/D_{30Surf} and σ_{SG}, which typically increase with bed slope) were weakly correlated with the reference shear stress in the total stress approach (Figure S1), but these correlations disappear when $\tau^{*\prime}_{rD50}$ is derived from the effective shear stress approaches (Figures S2 and S3).

Table 2. Hiding Function Parameters (τ^*_{ri}) and Exponents m_{i50} of Dimensionless Fractional Bed Load Rating Curves (W^*_i) Derived From Total Boundary Shear Stress τ^* and the Reduced Effective Shear Stress $\tau^{*\prime}$ According to *Rickenmann and Recking* [2011]

	Total Boundary Shear Stress				Effective Shear Stress (RR2011)			
	$\tau^*_{ri} = \tau^*_{rD50}(D_i/D_{50})^b$			$W^*_i = 0.002(\tau^*_i/\tau^*_{ri})^{mi50}$	$\tau^*_{ri} = \tau^*_{rD50}(D_i/D_{50})^b$			$W^{*\prime}_i = 0.002(\tau^{*\prime}_i/\tau^{*\prime}_{ri})^{mi50}$
Stream	τ^*_{rD50}	$-b$	r^2	m_{i50}	τ^*_{rD50}	$-b$	r^2	m_{i50}
Erlenbach	0.19	0.95	0.993	7.29	0.01	0.85	0.933	2.64
Riedbach	0.12	0.89	0.999	16.91	0.05	0.77	0.997	8.28
St. Louis Cr.	0.09	0.98	0.998	7.78	0.07	0.95	0.992	3.48
Cherry Cr.	0.12	0.96	1.000	21.45	0.06	0.92	0.998	11.02
Litl. Granite Cr. A	0.07	0.97	1.000	25.32	0.03	0.95	1.000	13.89
E. St. Louis Cr. A[a]								
E. St. Louis Cr. B	0.14	0.99	1.000	20.52	0.02	0.97	0.999	8.63
Halfmoon Cr.	0.09	0.97	0.999	10.65	0.04	0.91	0.997	5.70
Hayden Cr.	0.11	0.95	1.000	16.68	0.04	0.90	0.998	7.46
E. Dallas Cr.	0.06	0.85	0.999	13.67	0.03	0.70	0.997	6.82
Fool Cr.	0.07	0.98	1.000	32.02	0.02	0.97	0.999	13.31
NF Swan Cr.	0.15	1.08	0.996	6.50	0.05	1.16	0.984	3.08
Litl. Granite Cr. B	0.05	0.91	0.999	12.11	0.03	0.82	0.994	6.07
Oak Cr.	0.04	0.86	1.000	10.62	0.03	0.73	0.999	5.24
Big W. R. nr. Ket.	0.04	0.92	0.996	6.17	0.02	0.85	0.986	3.46
Boise R.	0.02	0.90	0.994	3.23	0.01	0.86	0.986	2.29
Dollar Cr.	0.05	0.92	0.996	4.65	0.02	0.80	0.977	2.06
Lochsa R.	0.03	0.84	0.996	6.42	0.02	0.78	0.991	4.82
MF Red R.	0.04	0.45	0.811	2.86	0.04	0.02	0.003	1.61
MF Salmon R.	0.03	0.93	0.997	11.84	0.02	0.91	0.994	8.65
NFCl. Water R.	0.01	1.06	0.994	5.79	0.01	1.08	0.993	4.85
Rapid R.	0.06	0.76	0.989	4.36	0.04	0.42	0.821	1.80
Salmon R. bl. Ynk. F	0.03	0.97	0.993	8.53	0.02	0.96	0.984	5.76
Salmon R. nr. Obs.	0.04	0.88	0.997	7.14	0.03	0.82	0.992	4.84
Salmon R. nr. Shp.	0.02	0.94	0.998	7.81	0.02	0.93	0.997	6.77
Selway R.	0.02	0.93	0.996	6.24	0.02	0.92	0.994	4.97
SF Payette R.	0.02	0.89	0.897	1.97	0.01	0.81	0.683	1.08
Squaw Cr. USGS	0.04	0.86	0.983	4.52	0.02	0.73	0.920	2.35
Thompson Cr.	0.05	0.82	0.994	6.57	0.03	0.61	0.946	2.95
Susitna R. nr. Talk.	0.02	1.03	0.897	2.75	0.02	1.03	0.879	2.50
Talkeetna R. nr. Talk.	0.01	0.74	0.972	3.86	0.01	0.73	0.969	3.72
Buffalo Cr.	0.01	0.90	0.996	5.47	0.01	0.89	0.995	5.17
Horse Cr.	0.02	0.63	0.977	5.31	0.01	0.37	0.828	3.07
Lo. SF Williams F.	0.07	0.79	0.937	4.33	0.02	0.41	0.337	1.55
Williams F.	0.02	0.84	0.989	6.70	0.01	0.67	0.933	3.25
Median Main-Data	0.09	0.96		13.67	0.03	0.91		6.82
Median HS-Data	0.03	0.88		5.39	0.02	0.81		3.16

[a]Only two full phi size fractions measured.

3.1.2. $\tau^*_{rD50tot}$—Derived From Total Bed Load Transport Rates

The dimensionless reference shear stress values $\tau^*_{rD50tot}$ derived from total bed load transport rates for $D > 4$ mm (see section 2.3.2 and Table 2) almost exactly correspond to the τ^*_{rD50} values derived from fractional transport rates for the Main Data set, but deviate somewhat for the HS Data set (Figures 3a and 3b). Also, the general trend of τ^*_{rD50} with channel slope for the Main Data set is not strongly affected by whether τ^*_{rD50} was derived from fractional or total transport rates (equations (9) and (10)).

$$\tau^*_{rD50tot} = 0.56S^{0.5};\ r^2 = 0.67 \text{ for } S > 0.01 \tag{10}$$

3.2. Hiding Exponent *b*

The dimensionless fractional reference shear stress for individual particle-size fractions τ^*_{ri} is related to the dimensionless reference shear stress of the median grain size τ^*_{rD50} through the power law hiding function and the hiding exponent b (equation (2)). The median hiding exponent b derived from the total boundary shear stress for the Main Data set is −0.96 (min: −0.85, max: −1.08) (Figure 4). The range of b derived from the effective shear stress (RR2011) for the Main Data set is similar to the total boundary stress case (median: −0.92, min: −0.72, max: −1.15). Median values of b for the HS Data set are generally lower and more scattered compared to the Main Data set b values (Figure 4).

Table 3. Dimensionless Fractional Bed Load Rating Curves for Total Bed Load Transport Rates > 4 mm Derived From Total Boundary Shear Stress τ^*_{D50} and the Reduced Effective Shear Stress $\tau^{*\prime}_{D50}$ According to *Rickenmann and Recking* [2011]

	Total Boundary Shear Stress			Effective Shear Stress		
	$W^*_{tot} = 0.002(\tau^*_{D50}/\tau^*_{rD50tot})^{mtot}$			$W^{*\prime}_{tot} = 0.002(\tau^{*\prime}_{D50}/\tau^*_{rD50tot})^{mtot}$		
Stream	$\tau^*_{rD50tot}$	m_{tot}	r^2	$\tau^*_{rD50tot}$	m_{tot}	r^2
Erlenbach	0.18	7.66	0.44	0.01	2.83	0.33
Riedbach	0.11	15.96	0.91	0.04	7.55	0.89
St. Louis Cr.	0.08	13.38	0.35	0.06	6.33	0.29
Cherry Cr.	0.11	24.93	0.88	0.06	12.92	0.87
Litl. Granite Cr. A	0.06	32.78	0.75	0.03	18.35	0.74
E. St. Louis Cr. A	0.13	22.61	0.75	0.02	9.60	0.72
E. St. Louis Cr. B	0.14	22.62	0.78	0.03	9.74	0.75
Halfmoon Cr.	0.08	16.31	0.76	0.04	7.65	0.72
Hayden Cr.	0.11	18.33	0.72	0.04	8.29	0.67
E. Dallas Cr.	0.06	12.69	0.75	0.03	6.14	0.71
Fool Cr.	0.08	27.44	0.38	0.02	12.26	0.35
NF Swan Cr.	0.16	9.31	0.22	0.08	3.94	0.17
Litl. Granite Cr. B	0.05	15.79	0.81	0.03	7.96	0.78
Oak Cr.	0.04	10.26	0.86	0.02	5.03	0.81
Big W. R. nr. Ket.	0.04	8.58	0.66	0.03	4.62	0.60
Boise R.	0.05	5.15	0.54	0.04	3.86	0.49
Dollar Cr.	0.08	4.92	0.30	0.06	1.90	0.18
Lochsa R.	0.03	8.00	0.58	0.03	6.19	0.55
MF Red R.	0.05	2.30	0.15	0.05	0.95	0.07
MF Salmon R.	0.03	16.07	0.66	0.03	12.04	0.66
NFCl. Water R.	0.02	8.34	0.71	0.02	7.17	0.69
Rapid R.	0.05	5.49	0.35	0.03	2.45	0.24
Salmon R. bl. Ynk. F	0.04	12.05	0.43	0.03	8.36	0.40
Salmon R. nr. Obs.	0.04	10.58	0.51	0.03	7.36	0.49
Salmon R. nr. Shp.	0.02	10.09	0.57	0.02	8.65	0.56
Selway R.	0.02	11.61	0.68	0.02	9.42	0.66
SF Payette R.	0.04	3.85	0.34	0.03	2.47	0.26
Squaw Cr. USGS	0.05	7.51	0.43	0.03	4.22	0.37
Thompson Cr.	0.06	6.38	0.46	0.03	2.85	0.35
Susitna R. nr. Talk.	0.03	6.46	0.47	0.03	6.01	0.46
Talkeetna R. nr. Talk.	0.01	5.15	0.59	0.01	4.90	0.59
Buffalo Cr.	0.01	5.57	0.51	0.01	5.27	0.51
Horse Cr.	0.01	4.42	0.38	0.00	2.49	0.30
Lo. SF Williams F.	0.07	5.80	0.58	0.03	2.31	0.45
Williams F.	0.02	9.40	0.67	0.01	4.64	0.61
Median Main-Data	0.09	16.14		0.03	7.81	
Median HS-Data	0.04	6.46		0.03	4.64	

Because the available bed load transport data pertain mainly to low and moderate flow conditions, almost no fractional bed load transport rates were measured for grain sizes larger than the D_{50Surf}. A comparison of b with the streambed characteristics described in section 3.1.1 can be found in the supporting information (Figures S4–S6).

3.3. Bed Load Transport Rating Curves

3.3.1. Fractional Bed Load Transport Rates

The dimensionless reference shear stress per grain-size fraction τ^*_{ri} derived in step (2) in section 2.3.2 was used to collapse fractional bed load transport rates computed from the total boundary shear stress approach and the effective shear stress approach according to RR2011 (equation (6)). Power law exponents m_i of collapsed fractional transport relations ($W^*_i = 0.002(\tau^*_i/\tau^*_{ri})^{mi}$) are much more variable among the different streams than for the individual grain-size classes of a specified stream (Figure 5). The median values of m_i of the size classes larger than 4 mm plot more or less on the same level for the Main data set (for the 2–4 mm size class data are available from the Oak Creek only). Because no systematic trends in m_i with grain-size class could be observed, the median exponent m_{i50} (see Figure 2c and Table 2 and Table S1) is used for fractional transport prediction. The nondimensional rating curves of the total boundary stress approach are significantly steeper ($m_{i50} = 13.7$, Main Data set only) than the exponent of 7.5 given in the *Wilcock and Crowe* [2003] equation. By comparison, the effective shear stress approach yields smaller rating curve

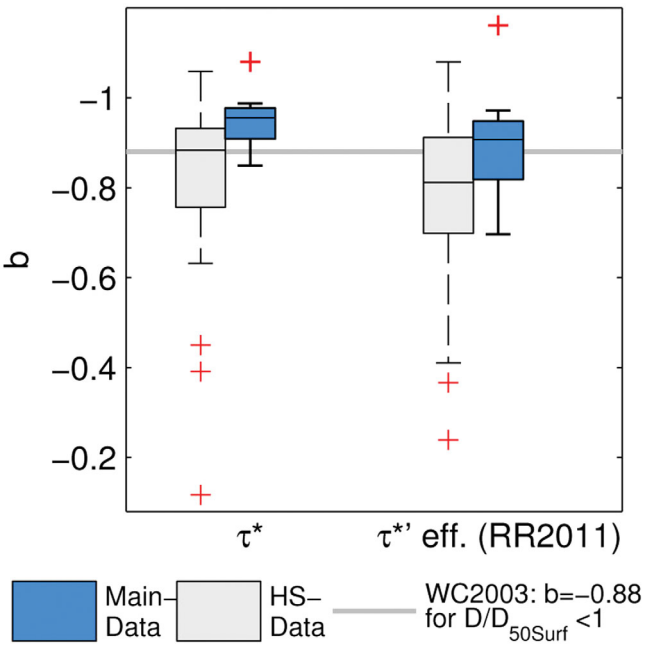

Figure 4. Boxplots of hiding exponent *b*, derived using total boundary shear stress τ^* and the reduced effective stress $\tau^{*\prime}$ (RR2011). Dark blue boxes are based on the Main Data set values including the bed load trap, vortex, and moving bed load basket data. Light gray boxes represent *b* values of the *Helley and Smith* data. Boxplot edges represent the 25th and 75th percentiles, whiskers include data within ±2.7 standard deviations, and outliers are presented as red crosses. The gray line represents the hiding exponent *b* as given by *Wilcock and Crowe* [2003] for $D < D_{50Surf}$.

exponents ($m_{i50} = 6.8$, Main Data set only), which are considerably closer to the *Wilcock and Crowe* [2003] exponent (Figures 5 and 6). Furthermore, the rating curve exponents m_i are generally higher for the Main Data set than for the HS Data set, for both the total boundary shear stress approach and the effective shear stress approach (Figures 5 and 6).

Figure 7 shows the collapsed fractional transport rates based on the dimensionless reference shear stress per grain-size fraction τ^*_{ri} for the total shear stress case and the effective shear stress $\tau^{*\prime}_{ri}$ (RR2011) case (see Figure S7 for WC2009). The dimensionless fractional transport rates W^*_i are a steeper function of total shear stress (Figure 7a) than the $W^{*\prime}_i$ are of effective shear stress (Figure 7b). The collapsed dimensionless $W^{*\prime}_i$ data (Figure 7a) appear to be less scattered than W^*_i (Figure 7b) for given values of τ^*_i/τ^*_{ri} or $\tau^{*\prime}_i/\tau^{*\prime}_{ri}$, respectively; however, this visual illusion is not confirmed when comparing observed and calculated dimensional transport rates presented later in the manuscript (equations (11) and (12), section 3.4 below). The very steep trends shown in Figures 7a and 7b are unlikely to continue at high shear stresses ($\tau^*_i/\tau^*_{ri} \gtrsim 1.3$), but may instead approach a constant value of W^*_i (and $W^{*\prime}_i$, respectively), as predicted by the *Wilcock and Crowe* [2003] equation. Because the trend is steep, the scatter in transport rates W^*_i (and $W^{*\prime}_i$, respectively) is huge (ranging 2 orders of magnitude above and below the WC2003 equation) while the scatter in τ^*_i/τ^*_{ri} is much smaller (roughly half an order of magnitude).

3.3.2. Total Bed Load Transport Rates

Nondimensional rating curves were also fitted for the total dimensionless bed load transport rates for both the total and effective-shear-stress (RR2011) approaches (Table 3 and Table S1 and Figures S8 and S9). The power law exponents m_{tot} for total transport rates are 14% – 47% higher than the exponents m_{i50} derived from the fractional rating curves (Figure 6). Otherwise, the behavior of m_{tot} is the same as for m_i: the m_{tot} values based on total boundary shear stress are higher than m_{tot} values derived from the effective shear stress, and the Main Data set m_{tot} values are generally higher than the HS Data set values (Figure 6).

3.4. Implications for Bed Load Transport Prediction

Our findings concerning the dimensionless reference shear stress, the relative size effects, and steepness of the bed load transport rating curves, as well as the effects of using total boundary shear stress or an effective shear stress, led us to set up dimensionless bed load transport models, similar to the original form of the *Wilcock and Crowe* [2003, hereinafter WC2003] equation. Rather than proposing an improved bed load transport equation for steep mountain streams, our main aim is to demonstrate how the effective shear stress estimate and the observed steep increase of bed load transport rates with increasing flow energy affect bed load transport prediction. The following six approaches were used for bed load transport prediction:

1. The original WC2003 equation (equations (A1–A4)) in combination with the *total* boundary shear stress (Figure 8a).

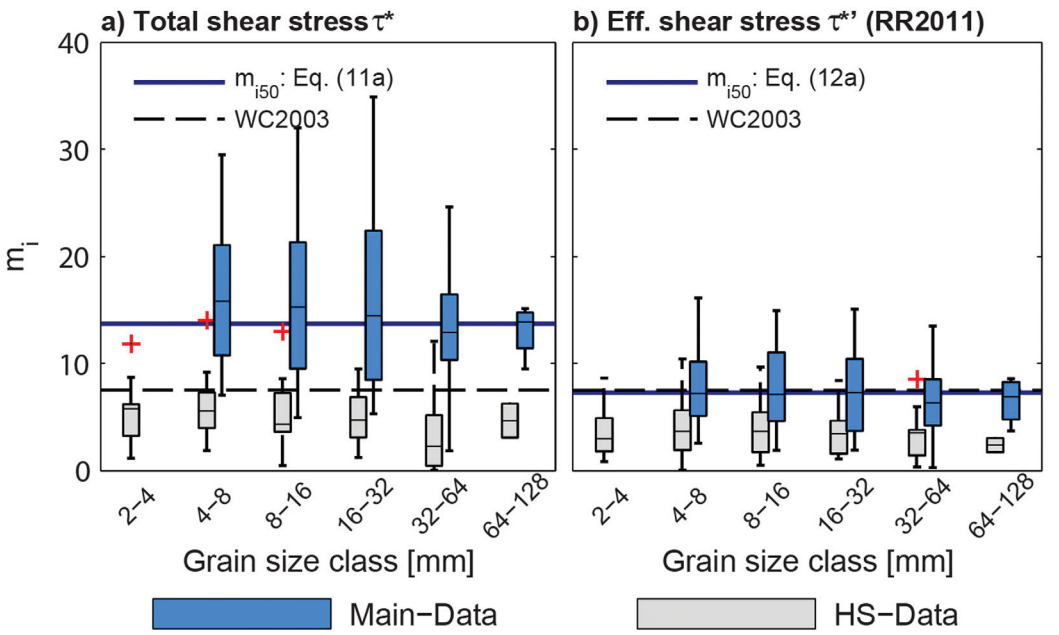

Figure 5. Boxplots of power law exponents m_i ($W_i^* = 0.002(\tau_i^*/\tau_{ri}^*)^{mi}$) related to grain size class, derived from the (a) total shear stress and (b) the effective shear stress according to *Rickenmann and Recking* [2011]. The blue thick lines represent the median exponent m_{i50} averaged over all grain size classes and streams of the Main Data set. The dashed lines represent the exponent given by *Wilcock and Crowe* [2003]. Boxplot edges represent the 25th and 75th percentiles, whiskers include data within ±2.7 standard deviations, and outliers are presented as red crosses. In the 2–4 mm class, no data points are available from the Main Data set.

2. The original WC2003 equation (equations (A1–A4)) in combination with the *effective* shear stress RR2011 (Figure 8b).

3. A modified WC2003 equation in combination with the *total* boundary shear stress, τ_{rD50}^* from equation (8), τ_{ri}^* from equation (A4) and a median exponent $m_{i50} = 13.7$ for the Main Data set for $\tau_i^*/\tau_{ri}^* < 1.2$ (equation (11); Figure 8c).

$$W_i^* = \begin{cases} 0.002\left(\tau_i^*/\tau_{ri}^*\right)^{13.7} & \text{for } \tau_i^*/\tau_{ri}^* < 1.2 \quad (11a) \\ 14\left(1 - \dfrac{0.85}{\left(\tau_i^*/\tau_{ri}^*\right)^{0.7}}\right)^{4.5} & \text{for } \tau_i^*/\tau_{ri}^* \geq 1.2 \quad (11b) \end{cases}$$

4. A modified WC2003 equation in combination with the *effective* shear stress RR2011, a constant dimensionless reference shear stress of $\tau_{rD50}^{*\prime} = 0.03$, $\tau_{ri}^{*\prime}$ from equation (A4), and a median exponent $m_{i50} = 6.8$ for the Main Data set for $\tau_i^{*\prime}/\tau_{ri}^{*\prime} < 1.33$ (equation (12); Figure 8d).

$$W_i^{*\prime} = \begin{cases} 0.002\left(\tau_i^{*\prime}/\tau_{ri}^{*\prime}\right)^{6.82} & \text{for } \tau_i^{*\prime}/\tau_{ri}^{*\prime} < 1.33 \quad (12a) \\ 14\left(1 - \dfrac{0.894}{\left(\tau_i^{*\prime}/\tau_{ri}^{*\prime}\right)^{0.5}}\right)^{4.5} & \text{for } \tau_i^{*\prime}/\tau_{ri}^{*\prime} \geq 1.33 \quad (12b) \end{cases}$$

5. A modified WC2003 equation calculating total transport rates in combination with the *total* boundary shear stress τ_{rD50}^* from equation (10) and a median exponent $m_{tot} = 16.1$ for the Main Data set for $\tau_{D50}^*/\tau_{rD50}^* < 1.2$ (equation (13), Figure 8e).

$$W_{tot}^* = \begin{cases} 0.002\left(\tau_{D50}^*/\tau_{rD50}^*\right)^{16.1} & \text{for } \tau_{D50}^*/\tau_{rD50}^* < 1.2 \text{ and } D > 4\,\text{mm} \quad (13a) \\ 14\left(1 - \dfrac{0.85}{\left(\tau_{D50}^*/\tau_{rD50}^*\right)^{0.7}}\right)^{4.5} & \text{for } \tau_{D50}^*/\tau_{rD50}^* \geq 1.2 \text{ and } D > 4\,\text{mm} \quad (13b) \end{cases}$$

6. A modified WC2003 equation calculating total transport rates in combination with the *effective* shear stress RR2011, a constant dimensionless reference shear stress of $\tau^{*\prime}_{rD50} = 0.03$, and a median exponent $m_{tot} = 7.8$ for the Main Data set for $\tau^{*\prime}_{D50}/\tau^{*\prime}_{rD50} < 1.33$ (equation (14), Figure 8f).

$$W^*_{tot} = \begin{cases} 0.002\left(\tau^{*\prime}_{D50}/\tau^{*\prime}_{rD50}\right)^{7.8} & \text{for } \tau^{*\prime}_{D50}/\tau^{*\prime}_{rD50} < 1.33 \text{ and } D > 4\,\text{mm} \quad (14a) \\ 14\left(1 - \dfrac{0.894}{\left(\tau^{*\prime}_{D50}/\tau^{*\prime}_{rD50}\right)^{0.5}}\right)^{4.5} & \text{for } \tau^{*\prime}_{D50}/\tau^{*\prime}_{rD50} \geq 1.33 \text{ and } D > 4\,\text{mm} \quad (14b) \end{cases}$$

For all fractional transport calculations, the hiding exponent of *Wilcock and Crowe* [2003] (equation (A4)) was used. The rationale for using modified *Wilcock and Crowe* [2003] equations, with two trends for $\tau^*_i/\tau^*_{ri} < 1.33$ and $\tau^*_i/\tau^*_{ri} \geq 1.33$, was based on the observation that dimensionless transport rates appear to asymptotically approach a constant value for high τ^*_i/τ^*_{ri}. Therefore, we kept the definition that W^*_i asymptotically approaches the value of 14, and we fitted the equations (11b) and (13b) for $\tau^*_i/\tau^*_{ri} \geq 1.33$ by eye to yield an appropriately shaped transport function (red lines, Figure 7).

We first calculated transport rates using the six different methods. Four were obtained by summing fractional transport rates derived from approaches (1)–(4) above; the other two were total bed load transport predictions based on approaches (5) and (6) above. The approach with the highest predictive accuracy (approach 4, equation (12)) was then used to present fractional transport rates for individual size classes ranging from 2 to128 mm. The predictive accuracy was defined by a score representing the percentage of data that fell within 1 order of magnitude of the measured (fractional or total) bed load transport rate (SC_{10}, $0.1 < q_{bcalc}/q_{bmeas} < 10$), and a second score representing the percentage within 3 orders of magnitude of the measured rate (SC_{1000}, $0.001 < q_{bcalc}/q_{bmeas} < 1000$), where q_{bcalc} is the computed bed load transport rate and q_{bmeas} is the measured unit bed load transport rate.

The predictive accuracy of total bed load transport rates (summed fractional rates) is lowest for the WC2003 approach coupled with an unreduced boundary shear stress (Figure 8a), and its inaccuracy increases with channel bed gradient (Figure 9a). Using the WC2003 equation in combination with an effective shear stress [*Rickenmann and Recking*, 2011; *Wilcock et al.*, 2009] significantly improves bed load transport predictions (Figure 8b and Figure S10a) and lessens slope-related overestimations (Figure 9b and Figure S11a), although predictions for the Main Data set streams in particular remain overestimated (Figure 8b). For all six models tested in Figure 8, the predictions derived from models calibrated to the field data (Main Data set) still display large scatter. However, bed load transport predictions that include corrections for macro-roughness (Figures 8d and 8f) tend to perform better compared to predictions based on the total boundary shear stress and the variable shear stress. No substantial differences could be observed between transport rates predicted from total and fractional transport calculations (Figure 8). Note that fractional transport rates for the Riedbach and Erlenbach were summed for size

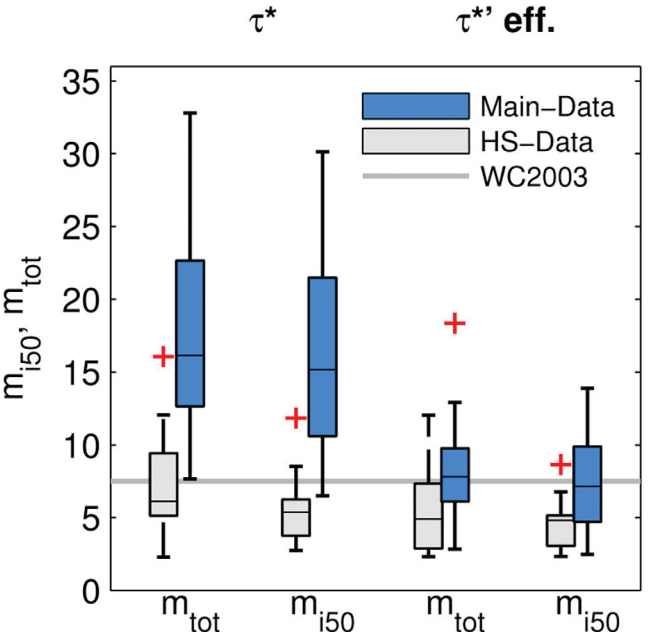

Figure 6. Boxplots of exponents m_{i50} (median of fractional exponents m_i) and m_{tot} of power laws fitted to collapsed dimensionless bed load transport rates ($W^*_i = 0.002\tau^*_i/\tau^{*mi}_{ri}$ and $W^*_{tot} = 0.002\tau^*_{D50Surf}/\tau^{*mtot}_{rD50Surf}$, respectively). The two left boxes are based on the total acting bed shear stress τ^*, and the two right boxes are based on the reduced effective acting bed shear stress $\tau^{*\prime}$ (RR2011). Dark blue boxes are based on the bed load trap, vortex, and moving bed load basket data. Light gray boxes represent *m* values of the *Helley and Smith* data. Boxplot edges represent the 25th and 75th percentiles, whiskers include data within ±2.7 standard deviations, and outliers are presented as red crosses.

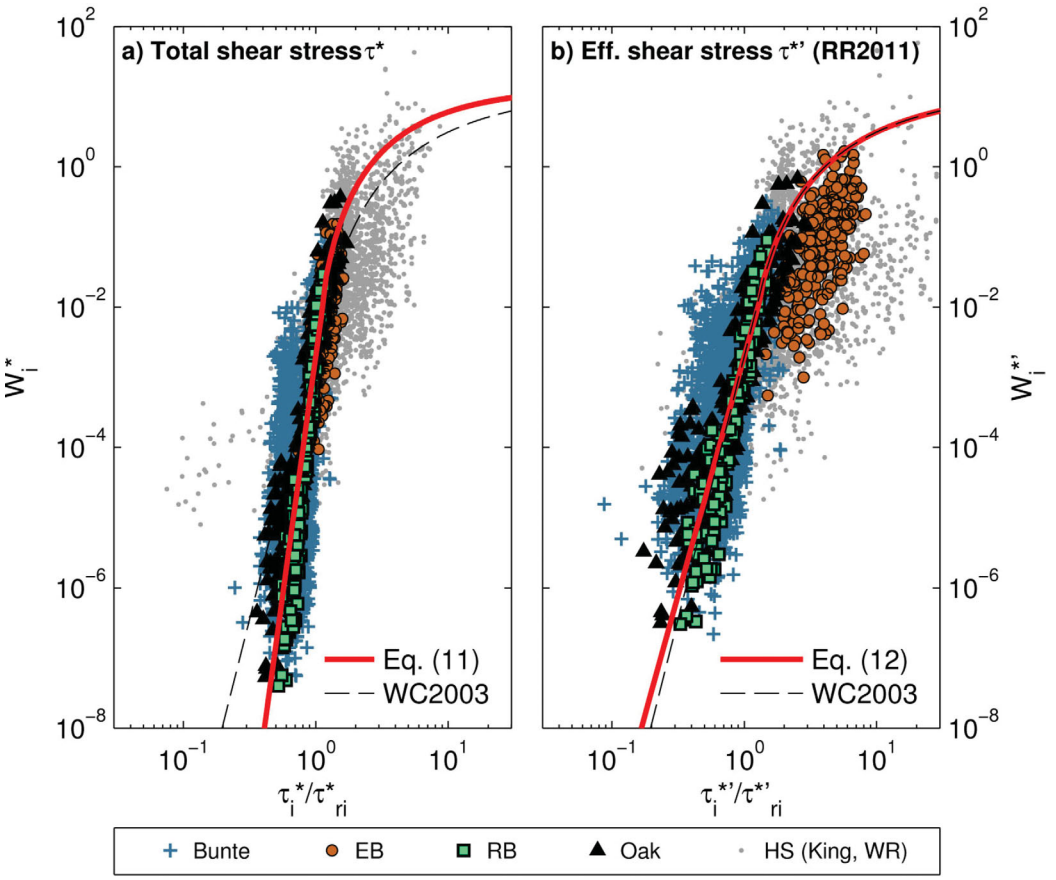

Figure 7. Similarity collapse of fractional transport rates based on τ_{ri}^* (derived from the reference approach of section 2.3.2, step (2)). (a) Collapse based on the total boundary shear stress τ^*. (b) Collapse based on the reduced effective bed shear stress $\tau^{*\prime}$ according to equation (6) [*Rickenmann and Recking* 2011].

fractions larger than the minimum sampled grain sizes of 6 and 10 mm, respectively. The expected error resulting from omitting fine gravel in those two cases decreases with increasing sampled transport rates and might amount to a factor of 2–5 for the smallest transport rate and a factor of <0.2 for the largest. These errors are negligible in the context of the analysis presented here. The predictive accuracy of fractional transport rates, based on approach (4) with a reduced effective shear stress, is generally similar among all considered grain-size classes, despite the fact that the uncalibrated *Wilcock and Crowe* [2003] hiding function was used (Figure 10).

4. Discussion

4.1. Effective Shear Stress and Threshold Shear Stress

The relationship between our calculated τ_{rD50}^* values and channel slope occupies a range similar to other reference and critical-stress relations (Figure 3a) [*Mueller et al*., 2005; *Lamb et al*., 2008]. However, we only found positive correlations between τ_{rD50}^* and channel slope, similar to those reported by *Mueller et al*. [2005] and *Lamb et al*. [2008], if τ_{rD50}^* was derived from total boundary shear stress. If, instead, an effective shear stress is used to compute $\tau_{rD50}^{*\prime}$ [*Rickenmann and Recking*, 2011; *Wilcock et al*., 2009], this positive trend disappears. Dimensionless reference shear stress values approach a median of $\tau_{rD50}^{*\prime} = 0.03$ for the Main Data set (Table 3 and Table S1), and the values vary in a similar range for both steep streams and for less steep channels, where effective shear stresses are much closer to total shear stresses [cf. *Recking*, 2009; *Yager et al*., 2012a].

It is obvious that macro-roughness limits the flow energy available for sediment transport at steep gradients, and it could also be shown based on both flume and field data that the energy needed for particle entrainment increases on steep beds [*Lamb et al*., 2008; *Mueller et al*., 2005; *Prancevic et al*., 2014; *Recking*, 2009]. However, it remains difficult to distinguish between these two effects—macro-roughness or threshold shear

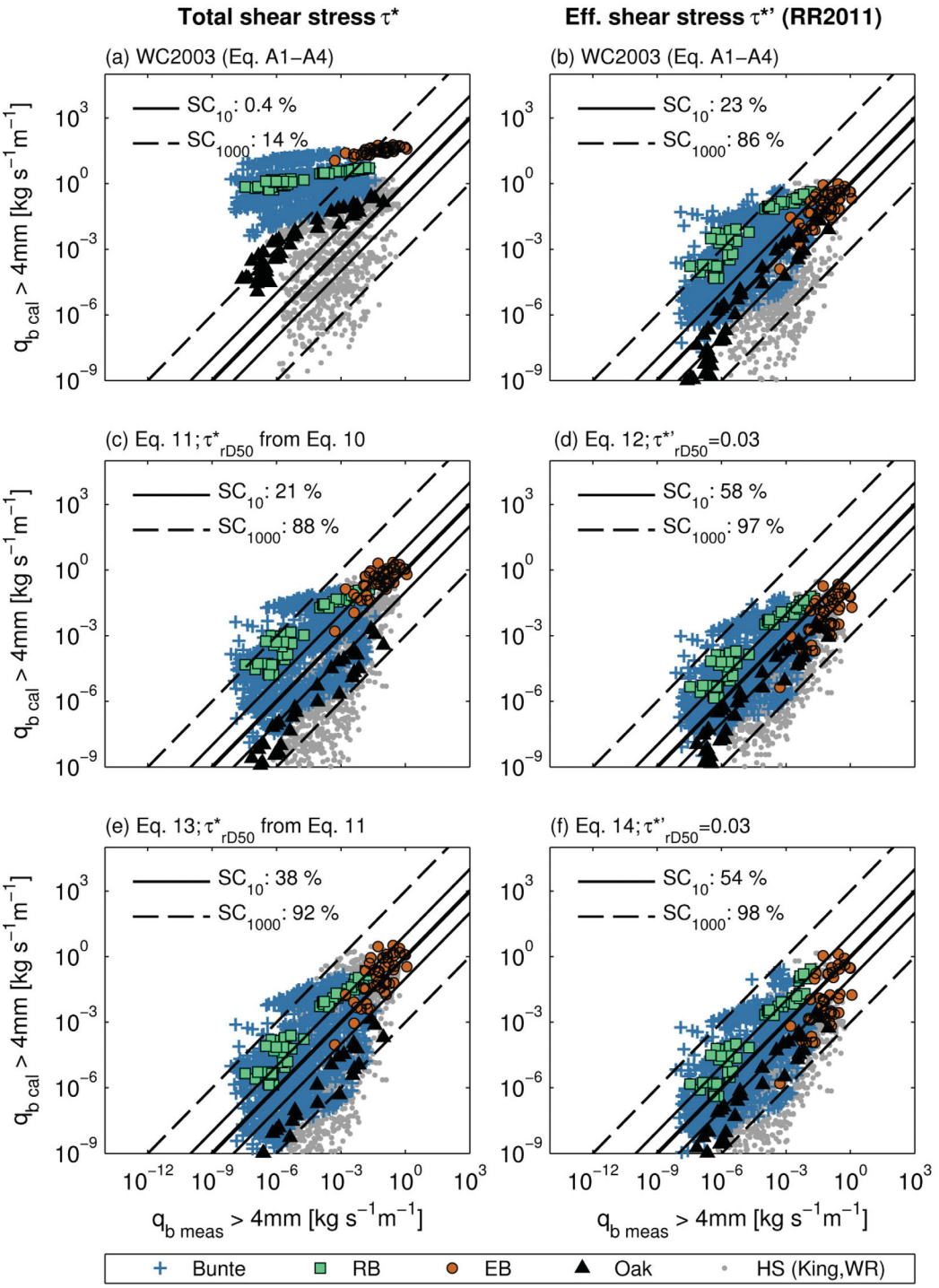

Figure 8. Bed load transport predictions ($D > 4$ mm) based on (left) the total acting bed shear stress τ^* and (right) the reduced effective acting bed shear stress $\tau^{*\prime}$ (RR2011) for (a and b) the *Wilcock and Crowe* [2003] equation; (c) equation (11) in combination with a dimensionless reference shear stress based on channel bed slope (equation (8)) derived from accumulated fractional calculations; (d) equation (12) in combination with a constant dimensionless reference shear stress $\tau^{*\prime}_{rD50} = 0.03$ derived from accumulated fractional calculations; (e) equation (13) in combination with a dimensionless reference shear stress based on channel bed slope (equation (9)) derived from total calculations; and (f) equation (14) in combination with a constant dimensionless reference shear stress $\tau^{*\prime}_{rD50} = 0.03$ derived from total calculations.

stress—because energy losses to macro-roughness will increase the fitted value of the reference shear stress in the *Parker et al.* [1982] approach [*Recking*, 2009]. For bed load transport prediction in steep streams, one commonly chooses either to reduce the total boundary shear stress [e.g., *Egashira and Ashida*, 1991; *Green et al.*, 2014; *Nitsche et al.*, 2011; *Pagliara and Chiavaccini*, 2006, *Rickenmann*, 2012; *Whittaker et al.*, 1990; *Yager et al.*,

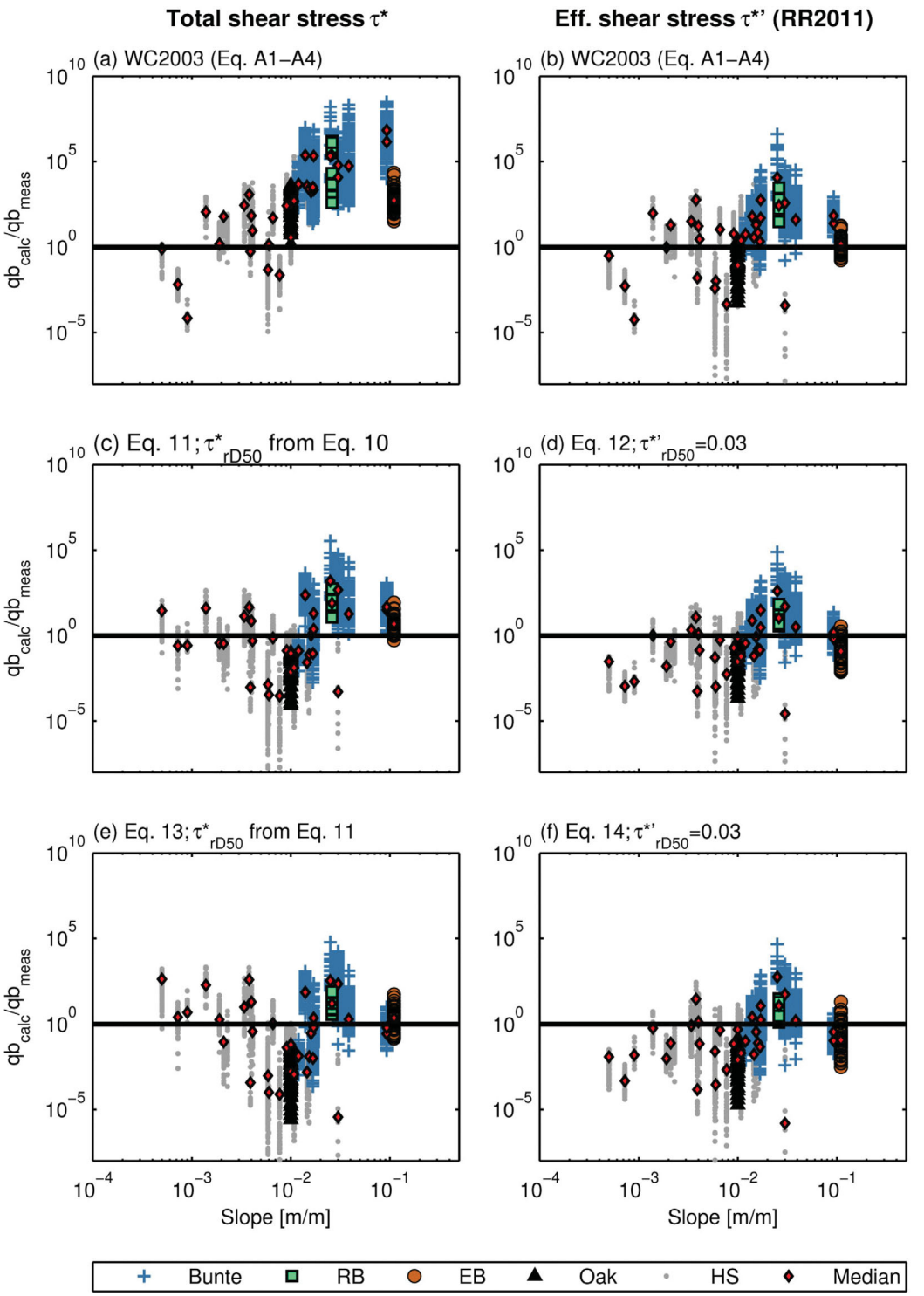

Figure 9. Discrepancy ratios (between calculated and measured unit transport rates) in relation to channel slope. Calculations are based on (left) the total acting bed shear stress τ^* and (right) the reduced effective acting bed shear stress $\tau^{*\prime}$ (RR2011) for (a and b) the *Wilcock and Crowe* [2003] equation; (c) equation (11) in combination with a dimensionless reference shear stress based on channel bed slope (equation (8)) derived from accumulated fractional calculations; (d) equation (12) in combination with a constant dimensionless reference shear stress $\tau^{*\prime}_{rD50} = 0.03$ derived from accumulated fractional calculations; (e) equation (13) in combination with a dimensionless reference shear stress based on channel bed slope (equation (9)) derived from total calculations; and (f) equation (14) in combination with a constant dimensionless reference shear stress $\tau^{*\prime}_{rD50} = 0.03$ derived from total calculations.

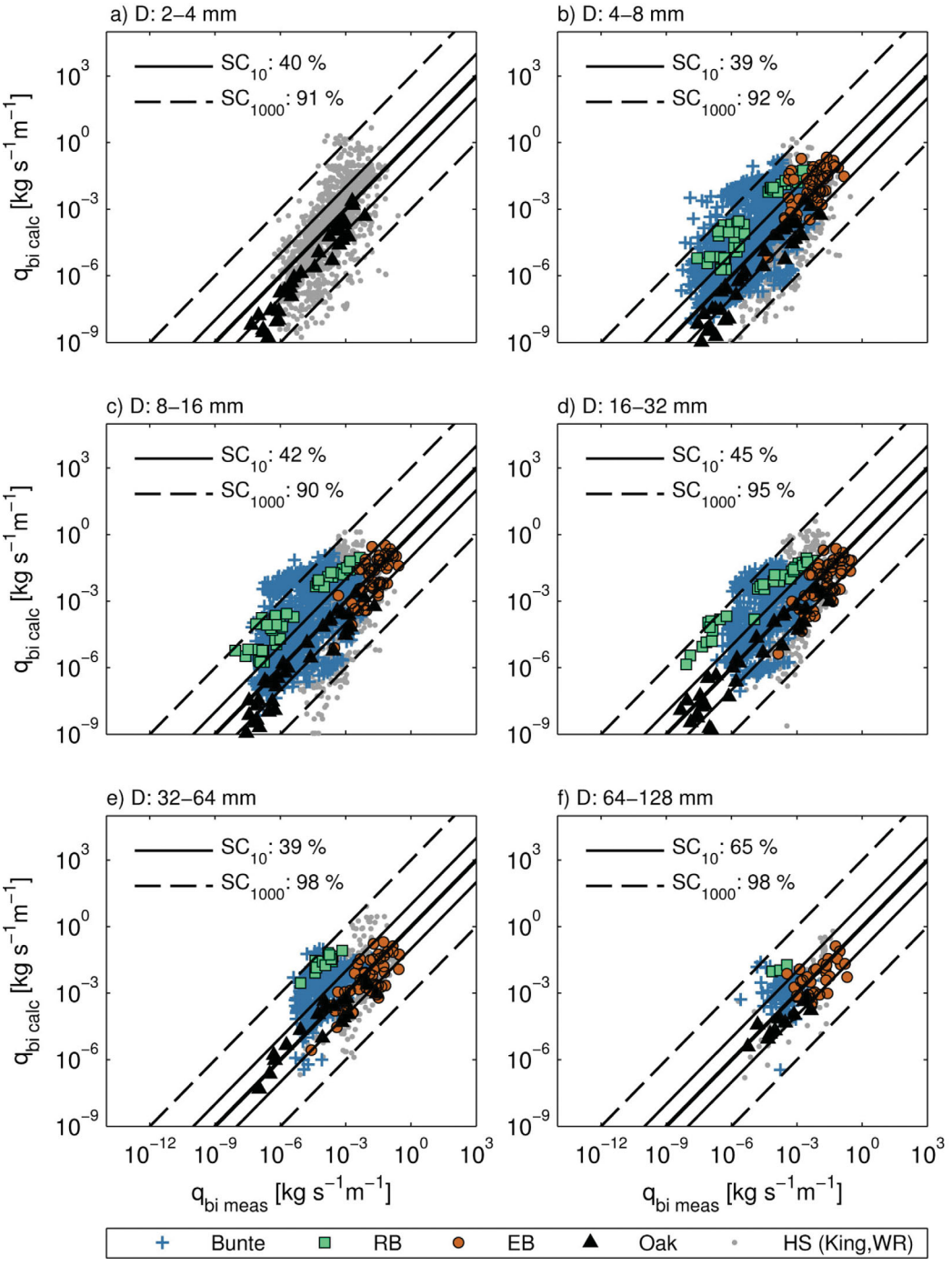

Figure 10. Fractional bed load transport prediction for grain size classes from (a) <4 mm to (f) <128 mm based on the effective shear stress approach RR2011 (equation (12)) in combination with a constant dimensionless reference shear stress $\tau^{*}_{rD50} = 0.03$. The hiding function used corresponds to equation (A4). In the 2–4 mm class, only data points from the HS Data set and Oak Creek are available.

2007, 2012b] or to increase the threshold shear stress [e.g., *Bunte et al.*, 2013; *Lamb et al.*, 2008; *Mueller et al.*, 2005; *Prancevic et al.*, 2014], to account for the reduced flow energy available and/or for the increased stability of bed particles. However, it was recently shown that the increase in critical shear stress with slope is not primarily related to increased particle friction angles and thus increased particle interlocking [*Prancevic and Lamb*, 2015b] but is mainly an effect of increased relative roughness [*Prancevic and Lamb*, 2015a], which correlates with channel slope in steep streams. This finding is in agreement with the reduced energy slope approach of *Rickenmann and Recking* [2011], which is mainly a function of relative flow depth.

Thus, the effective shear stress approach used here for bed load transport prediction does not necessarily contradict the observed increase in (total) threshold shear stress with channel slope. Based on the field data used here it is impossible to quantify the relative importance of the two factors. In natural steep channels both effects coincide, leading to reduced bed load transport rates at steep slopes under otherwise comparable hydraulic conditions.

4.2. Hiding Function Exponent *b*

The range of *b* found in this study is generally close to the values reported in the literature [e.g., *Andrews*, 1994; *Ashworth and Ferguson*, 1989; *Bathurst*, 2013; *Bunte et al*., 2013; *Ferguson*, 1994; *Gaeuman et al*., 2009; *Green et al*., 2014; *Mao et al*., 2008; *Parker*, 1990; *Recking*, 2009]. In contrast to the dimensionless reference shear stress τ^*_{rD50}, the hiding exponent *b* is not affected by using either the total boundary or the effective shear stress approach. This is not surprising because the shear stress reduction at steep slopes affects the dimensionless shear stress of all grain sizes in a similar way.

4.3. Dimensionless Bed Load Transport Rating Curves

The reason why the rating curve exponents m_i (and m_{i50}, respectively) and m_{tot} were smaller when based on effective rather than total boundary shear stress (Figure 7 and Figure S8) might not be intuitively apparent. This is because the range of τ^*/τ^*_r (both for fractional and total transport rates) is narrower for a given stream and a given flow discharge range when using a total shear stress as compared to an effective shear stress approach. Using equations (6) or (7) to reduce the total boundary shear stress, the $\tau^{*\prime}/\tau^{*\prime}_r$ ratio is also a function of relative flow depth (total boundary shear stress is reduced more strongly at shallower flows compared to deeper flows). By contrast, for the total boundary shear stress approach, the available flow energy τ^*/τ^*_r depends only on the absolute flow depth, but not on the relative flow depth.

Using the reduced shear stress approach, the median rating curve exponent $m_{i50} = 6.82$ is in much better agreement with the rating curve exponent of 7.5 obtained by *Wilcock and Crowe* [2003] experiments with nonuniform sediment. A somewhat similar finding comes from a study of *Recking* [2010] who developed an alternative transport equation that is also based on a reference shear stress. For τ^*/τ^*_r ratios smaller than about 1, he proposed a power law exponent $m = 12.9$ based on flume data with uniform bed material. For gravel-bed streams, which obviously have nonuniform grain-size distributions, he proposed an exponent of $m = 6.5$, and also introduced a correction function for the prefactor, which depends on channel slope and on the ratio D_{84}/D_{50}.

The larger m_i and m_{tot} exponents for the Main Data set streams, compared to the HS Data set streams (Figures 5 and 6), might be partly explained by uncertainties associated with the *Helley-Smith* (HS) bed load samples. *Bunte et al*. [2008] found that bed load transport rating curves determined with bed load traps are generally steeper than the rating curves determined from HS samplers. Whereas bed load transport rates measured with bed load traps increase steeply with discharge, bed load transport rates measured with HS samplers at the same sites yielded higher transport rates during low flow conditions and increased less steeply with discharge. The oversampling by the HS sampler at low flows has been attributed to short sampling times, to the flared HS sampler design, and to accidental particle pickup during sampler placement [*Bunte and Abt*, 2005].

The assumption made in this study, that dimensionless transport rates W^*_i tend to approach a constant value for high τ^*_i/τ^*_{ri} values (Figure 7), is only supported by a few data points. However, several studies, mainly using flume data [*Diplas and Shaheen*, 2007; *Meyer-Peter and Mueller*, 1948; *Parker*, 1990; *Rickenmann*, 1991; *Wilcock and Crowe*, 2003], have shown that transport observations asymptotically approach a relation $q_b^* \sim (\tau^*)^{1.5}$ for high shear stresses τ^*/τ^*_r, with a prefactor (coefficient) in the range of about 4–14 [*Wilcock and Crowe*, 2003; *Wong and Parker*, 2006; *Wilson*, 1987].

4.4. Bed Load Transport Prediction

Among the six versions of the *Wilcock and Crowe* [2003] transport model compared in this study, the original approach (WC2003) that employs an unreduced boundary shear stress (Figure 8a) had the lowest predictive accuracy. This is not surprising, because the equation was not developed for steep streams; it does not take potential energy losses into account and thus tends to overestimate bed load transport rates, especially in steep streams (Figure 9a). Using the WC2003 equation in combination with an effective shear stress, as in *Rickenmann and Recking* [2011], significantly improves bed load transport predictions and lessens overestimations on steep slopes (Figures 8b and 9b).

The predictions of the modified WC2003 equations (equations 11–14; Figures 8c–8f) are still greatly scattered; however, using a reduced effective shear stress and a constant reference shear stress (equations 12 and 14; Figures 8d and 8f) results in slightly better bed load transport predictions than using the total boundary shear stress and the variable dimensionless reference shear stress from equations (11) and (13). Transport rates that were predicted based on total or fractional bed load transport calculations did not substantially differ.

The predictive accuracy of the individual grain-size fractions according to equation (12) and the *Wilcock and Crowe* [2003] hiding function (equation (A4)), is generally similar for all the considered grain-size classes (Figure 9), even if the hiding equation is not calibrated to the field data. It appears that the general issue of how to determine the governing shear stress and reference/critical shear stress, over wide ranges of bed gradients, plays a more significant role for bed load transport than for potential grain-size interactions. This also explains why the predictive accuracies of the fractional (Figures 8c and 8d) and the total (Figures 8e and 8f) bed load transport equations are generally comparable to each other.

Well after being fitted to field data, fractional transport models have a significant advantage in practical applications. Because the minimum grain sizes measured in the field can vary significantly depending on the measurement technique (e.g., from 0.25 mm in the King data set to 10 mm at the Erlenbach), it can be difficult to calibrate total bed load transport equations across data sets that combine different methods. Fractional transport models have the advantage that they do not depend on the minimum measured grain size, under assumption that the fractional rating curve exponents (m_i) are roughly constant with grain size (cf. Figure 5). Thus, fractional transport models can potentially be applied outside the range of grain sizes that are available for calibration in a field data set.

Although correcting for macro-roughness improves bed load transport predictions (Figures 8c–8f), the uncertainties in predicted transport rates remain huge (up to roughly 3 orders of magnitude), especially considering that these equations have been fitted to the field data (and thus do not represent a priori predictions). The large uncertainties indicate either that the measured data are very noisy, or that important processes or parameters are missing from all bed load transport equations. Variability in measured transport rates is likely, given the difficulties of measuring transport rates and flow conditions that vary greatly in both time and space. However, we assume that the bed load trap, moving basket, and vortex trap measurements yield some of the most accurate field data currently available for steep streams. Furthermore, in the simple transport calculations presented in this study, which focus on the estimation of the effective and reference shear stress over wide ranges of bed gradients, other important parameters driving bed load are neglected. For example, the effects of catchment, streambed, flow, and bed load transport characteristics on reference shear stress [e.g., *Efthymiou*, 2012; *Gaeuman et al*., 2009], hiding exponents [*Green et al*., 2014; *Mao et al*., 2008], and bed load rating curves [e.g., *Barry*, 2004; *Bunte et al*., 2015; *Diplas and Shaheen*, 2007; *Recking*, 2010] were not considered in this study. Furthermore, we have not considered sediment supply issues [e.g., *Bathurst*, 2007; *Recking*, 2012; *Yager et al*., 2012b]. These factors might explain some of the remaining deviations between predicted and observed transport rates.

5. Conclusions

Using a broad range of field data sets, we showed that transport equations such as the *Wilcock and Crowe* [2003] equation, which were developed on flume data for lower stream gradients, can also be applied to steep mountain streams if one accounts for flow resistance due to macro-roughness and/or the increased (total) shear stress for initiation of motion.

From our field data, it remains unclear how much of the flow energy available for bed load transport is lost due to flow resistance on macro-roughness elements in steep mountain streams, and how much more energy is needed for entrainment of particles from structurally stable positions on the bed. Fortunately, for bed load prediction itself, it matters little whether one reduces the flow energy available using a flow resistance equation, or whether one increases the critical threshold for particle entrainment (see Figures 8c–8f). Both approaches correct the available energy in the same direction (cf. Figure 1) and avoid the systematic overestimation of sediment transport rates that otherwise occurs in steep mountain streams [e.g., *Bathurst et al*., 1987; *Chiari and Rickenmann*, 2011; *Lenzi et al*., 1999; *Rickenmann*, 2001, 2012; *Yager et al*., 2007, 2012a]. However, selecting one approach over the other has implications for bed load transport predictions, because the stress-dependent increase in bed load transport rates defined by the power law exponents m_i strongly depends on which of the two approaches is

used. It is interesting that the power law exponents of 6.8 obtained from using the effective shear stress according to *Rickenmann and Recking* [2011] and *Wilcock et al*., [2009], are, on average for the Main Data set streams, close to the exponent of 7.5 given in the *Wilcock and Crowe* [2003] equation designed for lower bed gradients. This similarity in exponents allows the *Wilcock and Crowe* [2003] equation to be used, in combination with an effective shear stress approach, in steep mountain streams without substantial changes to the bed load transport relation, as would be necessary when using a reference shear stress that depends on channel slope.

Finally, bed load transport predictions do not significantly vary depending on whether they are derived from calculating transport rates for individual grain fractions, or from calculating total transport. It appears that compared to the variability of reference or critical shear stress and the effects of macro-roughness on transport efficiency (and their associated uncertainties), hiding and exposure effects are relatively insignificant, and the use of an average hiding exponent (equation (A4)) generally works well for fractional bed load transport prediction.

Appendix A: Wilcock and Crowe [2003] Equation

The *Wilcock and Crowe* [2003] equation is based on flume measurements that cover wide ranges of flows, transport rates, and bed surface sediments. The model is based on previous surface-based transport models [*Parker*, 1990; *Proffitt and Sutherland*, 1983]; however, its hiding function incorporates a nonlinear effect of sand content on gravel transport rates [*Wilcock et al*., 2001]. The dimensionless fractional transport rate W_i^* is defined as a function of $\theta_d = \tau/\tau_{ri}$.

$$W_i^* = \begin{cases} 0.002{\theta_d}^{7.5} & \text{for } \theta_d < 1.35 \quad \text{(A1a)} \\ 14\left(1-\dfrac{0.894}{{\theta_d}^{0.5}}\right)^{4.5} & \text{for } \theta_d \geq 1.35 \quad \text{(A1b)} \end{cases}$$

The reference shear stress τ_{ri} of each grain size fraction is determined using a dimensional form of a hiding function (equivalent to equation (1)), with its input parameters $\tau_{r50} = \tau_{rDm}$ and b' (note, b' in the dimensional form of the hiding function corresponds to $1 - b$).

$$\tau_{ri} = \tau_{rDm}\left(\frac{D_i}{D_m}\right)^{b'} \quad \text{(A2)}$$

$$\tau^*_{rD50} = (0.021 + 0.015\exp\left[-20F_s\right])(\rho_s - \rho)gD_{50Surf} \quad \text{(A3)}$$

$$b' = \frac{0.67}{1+\exp\left(1.5-\frac{D_i}{D_{50Surf}}\right)} \quad \text{(A4)}$$

where F_s is the proportion of sand in surface size distribution, D_i is the grain size of fraction i, and D_{50Surf} is the D_{50} of the streambed surface.

Acknowledgments
This study was supported by the CCES project APUNCH of the ETH domain, and partly by SNF grant 200021_124634/1 to D.R. The long-term field data collection with bed load traps in the U.S. was supported by the Stream Systems Technology Center (now National Stream and Aquatic Ecology Center) of the USDA Forest Service, Fort Collins, CO, USA. We thank K. Swingle, B. Schmid, N. Federspiel, and K. Steiner for field assistance. We thank A. Recking, E. Yager, and an anonymous reviewer for their constructive comments that helped to improve this paper. Please contact the authors if you are interested in the Swiss bed load data (D.R.).

References

Andrews, E. D. (1994), Marginal bed load transport in a gravel bed stream, Sagehen Creek, California, *Water Resour. Res.*, *30*(7), 2241–2250, doi:10.1029/94WR00553.

Andrews, E. D., G. Parker, C. R. Thorne, J. C. Bathurst, and R. D. Hey (1987), Formation of a coarse surface layer as the response to gravel mobility, in *Sediment Transport in Gravel-Bed Rivers*, edited by C. R. Thorne, J. C. Bathurst, and R. D. Hey, pp. 269–325, John Wiley, Chichester, U. K.

Ashida, K., and M. Michiue (1973), Study on bed load transport rate in open channel flows, paper presented at International Symposium on River Mechanics, Int. Assoc. for Hydraul. Res., Bangkok.

Ashworth, P. J., and R. I. Ferguson (1989), Size-selective entrainment of bed load in gravel bed streams, *Water Resour. Res.*, *25*(4), 627–634, doi:10.1029/WR025i004p00627.

Barry, J. J. (2004), A general power equation for predicting bed load transport rates in gravel bed rivers, *Water Resour. Res.*, *40*, W10401, doi:10.1029/2004WR003190.

Barry, J. J., J. Buffington, P. Goodwin, J. King, and W. Emmett (2008), Performance of bed-load transport equations relative to geomorphic significance: Predicting effective discharge and its transport rate, *J. Hydraul. Eng.*, *134*(5), 601–615, doi:10.1061/(ASCE)0733-9429(2008)134:5(601).

Bathurst, J. C. (2007), Effect of coarse surface layer on bed-load transport, *J. Hydraul. Eng.*, *133*(11), 1192–1205, doi:10.1061/(ASCE)0733-9429(2007)133:11(1192).

Bathurst, J. C. (2013), Critical conditions for particle motion in coarse bed materials of nonuniform size distribution, *Geomorphology*, *197*, 170–184, doi:10.1016/j.geomorph.2013.05.008.

Bathurst, J. C., W. H. Graf, and H. H. Cao (1987), Bed load discharge equations for steep mountain rivers, in *Sediment Transport in Gravel-Bed Rivers*, edited by C. R. Thorne, J. C. Bathurst, and R. D. Hey, pp. 453–477, John Wiley, N. Y.

Bettess, R. (1984), Technical note. Initiation of sediment transport in gravel bed streams, in *ICE Proceedings*, vol. 77, Thomas Telford, London, U. K., doi:10.1680/iicep.1984.1275.

Buffington, J. M., and D. R. Montgomery (1997), A systematic analysis of eight decades of incipient motion studies, with special reference to gravel-bedded rivers, *Water Resour. Res.*, *33*(8), 1993–2029, doi:10.1029/96WR03190.

Bunte, K., and S. R. Abt (2001a), Sampling surface and subsurface particle-size distributions in wadable gravel-and cobble-bed streams for analyses in sediment transport, hydraulics, and streambed monitoring, *Gen. Tech. Rep*. RMRS-GTR-74, 428 pp., U.S. Dep. of Agric., For. Serv., Fort Collins, Colo.

Bunte, K., and S. R. Abt (2001b), Sampling frame for improving pebble count accuracy in coarse gravel-bed streams, *J. Am. Water Resour. Assoc.*, *37*(4), 1001–1014, doi:10.1111/j.1752-1688.2001.tb05528.x.

Bunte, K., and S. R. Abt (2005), Effect of sampling time on measured gravel bed load transport rates in a coarse-bedded stream, *Water Resour. Res.*, *41*, W11405, doi:10.1029/2004WR003880.

Bunte, K., S. R. Abt, J. P. Potyondy, and S. E. Ryan (2004), Measurement of coarse gravel and cobble transport using portable bedload traps, *J. Hydraul. Eng.*, *130*(9), 879–893, doi:10.1061/(ASCE)0733-9429(2004)130:9(879).

Bunte, K., K. W. Swingle, and S. R. Abt (2007), Guidelines for using bedload traps in coarse-bedded mountain streams: Construction, installation, operation and sample processing, *Gen. Tech. Rep*. RMRS-GTR-191, 91 pp., U.S. Dep. of Agric., For. Serv., Rocky Mt. Res. Stn., Fort Collins, Colo. [Available at http://www.fs.fed.us/rm/pubs/rmrs_gtr191.pdf.]

Bunte, K., S. R. Abt, J. P. Potyondy, and K. W. Swingle (2008), A comparison of coarse bedload transport measured with bedload traps and Helley-Smith samplers, *Geodin. Acta*, *21*(1–2), 53–66, doi:10.3166/ga.21.53-66.

Bunte, K., S. R. Abt, J. P. Potyondy, and K. W. Swingle (2009), Comparison of three pebble count protocols (EMAP, PIBO, and SFT) in two mountain gravel-bed streams1, *J. Am. Water Resour. Assoc.*, *45*(5), 1209–1227, doi:10.1111/j.1752-1688.2009.00355.x.

Bunte, K., S. R. Abt, K. W. Swingle, D. A. Cenderelli, and J. M. Schneider (2013), Critical Shields values in coarse-bedded steep streams, *Water Resour. Res.*, *49*, 7427–7447, doi:10.1002/2012WR012672.

Bunte, K., S. R. Abt, K. W. Swingle, and D. A. Cenderelli (2014), Effective discharge in Rocky Mountain headwater streams, *J. Hydrol.*, *519*, Part B, 2136–2147, doi:10.1016/j.jhydrol.2014.09.080.

Bunte, K., S. R. Abt, K. W. Swingle, D. A. Cenderelli, D. Rickenmann, and D. Gaeuman (2015), Scaling relations of exponents and coefficients for bedload transport and flow competence curves in coarse-bedded streams with channel gradient, runoff yield, basin area, and subsurface fines, paper presented at SEDHYD, joint 10th Federal Interagency Sedimentation and 5th Federal Interagency Hydraulic Modelling Conference, Fed. Interagency Sedimentation and 5th Fed. Interagency Hydraul. Modell., Reno, Nev., 19–23 April.

Carson, M. A. (1987), Measures of flow intensity as predictors of bed load, *J. Hydraul. Eng.*, *113*(11), 1402–1420, doi:10.1061/(ASCE)0733–9429(1987)113:11(1402).

Carson, M. A., and G. A. Griffiths (1987), Influence of channel width on bed load transport capacity, *J. Hydraul. Eng.*, *113*(12), 1489–1508, doi:10.1061/(ASCE)0733–9429(1987)113:12(1489).

Chiari, M., and D. Rickenmann (2011), Back-calculation of bedload transport in steep channels with a numerical model, *Earth Surf. Processes Landforms*, *36*(6), 805–815, doi:10.1002/esp.2108.

Chiari, M., K. Friedl, and D. Rickenmann (2010), A one-dimensional bedload transport model for steep slopes, *J. Hydraul. Res.*, *48*(2), 152–160, doi:10.1080/00221681003704087.

Diplas, P., and H. Shaheen (2007), 11 Bed load transport and streambed structure in gravel streams, in *Gravel-Bed Rivers VI: From Process Understanding to River Restoration*, edited by H. P. H. Habersack, H. Piégay, and M. Rinaldi, pp. 291–308, Elsevier, St. Jakob, Austria, doi: 10.1016/S0928–2025(07)11128-7.

Efthymiou, N. P. (2012), Transient bedload transport of sediment mixtures under disequilibrium conditions—An experimental study and the development of a new dynamic hiding function, PhD dissertation, Tech. Univ. München, München, Germany. [Available at http://www.wb.bv.tum.de/fileadmin/w00boi/www/Publikationen/Berichtshefte/Band126.pdf.]

Egashira, S., and K. Ashida (1991), Flow resistance and sediment transportation in streams with step-pool bed morphology, in *Fluvial Hydraulics of Mountain Regions*, edited by A. Armanini and G. Silvio, pp. 45–58, Springer, Berlin.

Egiazaroff, I. V. (1965), Calculation of nonuniform sediment concentrations, *J. Hydraul. Div. Am. Soc. Civ. Eng.*, *91*(HY4), 225–247.

Einstein, H. A. (1950), The bed-load function for sediment transportation in open channel flows, *Tech. Bull. 1026*, 71 pp., U.S. Dep. of Agric., Washington, D. C.

Emmett, W. W. (1980), *A Field Calibration of the Sediment-Trapping Characteristics of the Helley-Smith Bedload Sampler, U.S. Geol. Surv. Prof. Pap. 1139*, U.S. Gov. Print. Off., Washington, D. C. [Available at http://pubs.usgs.gov/pp/1139/report.pdf.]

Ferguson, R. (2007), Flow resistance equations for gravel- and boulder-bed streams, *Water Resour. Res.*, *43*, W05427, doi:10.1029/2006WR005422.

Ferguson, R. I. (1994), Critical discharge for entrainment of poorly sorted gravel, *Earth Surf. Processes Landforms*, *19*(2), 179–186, doi: 10.1002/esp.3290190208.

Ferguson, R. I. (2012), River channel slope, flow resistance, and gravel entrainment thresholds, *Water Resour. Res.*, *48*, W05517, doi:10.1029/2011WR010850.

Gaeuman, D., E. D. Andrews, A. Krause, and W. Smith (2009), Predicting fractional bed load transport rates: Application of the Wilcock-Crowe equations to a regulated gravel bed river, *Water Resour. Res.*, *45*, W06409, doi:10.1029/2008WR007320.

Gomez, B., and M. Church (1989), An assessment of bed-load sediment transport formulas for gravel bed rivers, *Water Resour. Res.*, *25*(6), 1161–1186, doi:10.1029/WR025i006p01161.

Green, K., Y. Alila, and F. Brardinoni (2015), Patterns of bedload entrainment and transport in forested headwater streams of the Columbia Mountains, Canada, *Earth Surf. Processes Landforms*, *40*, 427–446, doi:10.1002/esp.3642.

Helley, E. J., and W. Smith (1971), Development and calibration of a pressure-difference bedload sampler, *Open File Rep. 73–108*, U.S. Geol. Surv., Menlo Park, Calif. [Available at http://pubs.usgs.gov/of/1973/0108/report.pdf.]

Hunziker, R. P., and M. N. R. Jaeggi (2002), Grain sorting processes, *J. Hydraul. Eng.*, *128*(12), 1060–1068, doi:10.1061/(ASCE)0733–9429(2002)128:12(1060).

King, J. G., W. W. Emmett, P. J. Whiting, R. P. Kenworthy, and J. J. Barry (2004), Sediment transport data and related information for selected gravel-bed streams and rivers in Idaho, *Gen. Tech. Rep. RMRS-GTR-131*, 26 pp., U.S. Dep. of Agric., For. Serv., Fort Collins, Colo. [Available at www.fs.fed.us/rm/pubs/rmrs_gtr131.pdf.]

Klingeman, P. C. (1979), Sediment transport research facilities, Oak Creek, Oregon, *Oak Creek Sediment Transp. Rep. F1*, 24 pp., Oreg. Water Resour. Res. Inst., Oreg. State Univ., Corvallis.

Lamb, M. P., W. E. Dietrich, and J. G. Venditti (2008), Is the critical Shields stress for incipient sediment motion dependent on channel-bed slope?, *J. Geophys. Res.*, *113*, F02008, doi:10.1029/2007JF000831.

Lenzi, M. A., V. D'Agostino, and P. Billi (1999), Bedload transport in the instrumented catchment of the Rio Cordon Part I: Analysis of bedload records, conditions and threshold of bedload entrainment, *Catena*, *36*(3), 171–190, doi:10.1016/s0341–8162(99)00016-8.

Mao, L., G. P. Uyttendaele, A. Iroumé, and M. A. Lenzi (2008), Field based analysis of sediment entrainment in two high gradient streams located in Alpine and Andine environments, *Geomorphology*, *93*(3–4), 368–383, doi:10.1016/j.geomorph.2007.03.008.
Meyer-Peter, E., and R. Mueller (1948), Formulas for bedload transport, in *Proceedings of the* 2nd Meeting of *the International Association for Hydraulic Structures Research*, pp. 39–64, Int. Assoc. for Hydraul. Struct. Res., Stockholm.
Milhous, R. T. (1973), Sediment transport in a gravel-bottomed stream, PhD thesis, 232 pp., Oregon State Univ., Corvallis.
Millar, R. G. (1999), Grain and form resistance in gravel-bed rivers, *J. Hydraul. Res.*, *37*(3), 303–312.
Millar, R., and M. Quick (1994), Flow resistance of high-gradient gravel channels, paper presented at Conference of Hydraulic Engineering, ASCE, N. Y.
Montgomery, D. R., and J. M. Buffington (1997), Channel-reach morphology in mountain drainage basins, *Geol. Soc. Am. Bull.*, *109*(5), 596–611, doi:10.1130/0016–7606(1997)109<0596:CRMIMD>2.3.CO;2.
Mueller, E. R., J. Pitlick, and J. M. Nelson (2005), Variation in the reference shields stress for bed load transport in gravel-bed streams and rivers, *Water Resour. Res.*, *41*, W04006, doi:10.1029/2004WR003692.
Muskatirovic, J. (2008), Analysis of bedload transport characteristics of Idaho streams and rivers, *Earth Surf. Processes Landforms*, *33*(11), 1757–1768, doi:10.1002/esp.1646.
Nitsche, M., D. Rickenmann, J. M. Turowski, A. Badoux, and J. W. Kirchner (2011), Evaluation of bedload transport predictions using flow resistance equations to account for macro-roughness in steep mountain streams, *Water Resour. Res.*, *47*, W08513, doi:10.1029/2011WR010645.
Nitsche, M., D. Rickenmann, J. W. Kirchner, J. M. Turowski, and A. Badoux (2012), Macro-roughness and variations in reach-averaged flow resistance in steep mountain streams, *Water Resour. Res.*, *48*, W12518, doi:10.1029/2012WR012091.
Pagliara, S., and P. Chiavaccini (2006), Flow resistance of rock chutes with protruding boulders, *J. Hydraul. Eng.*, *132*(6), 545–552, doi:10.1061/(ASCE)0733-9429(2006)132:6(545).
Palt, S. M. (2001), Sediment transport prozesse im Himalaya-Karakorum und ihre Bedeutung für Wasserkraftanlagen, PhD thesis, Univ. Karlsruhe, Karlsruhe, Germany. [Available at http://nbn-resolving.org/urn:nbn:de:swb:90-AAA47120011.]
Parker, G. (1990), Surface-based bedload transport relation for gravel rivers, *J. Hydraul. Res.*, *28*(4), 417–436, doi:10.1080/00221689009499058.
Parker, G. (2008), Transport of gravel and sediment mixtures, in *ASCE Manual 54-Sedimentation Engineering: Processes, Measurements, Modeling, and Practice*, edited by M. H. Garcia, 162 pp., ASCE, Reston, Va, doi:10.1061/9780784408148.ch03.
Parker, G., and P. C. Klingeman (1982), On why gravel bed streams are paved, *Water Resour. Res.*, *18*(5), 1409–1423, doi:10.1029/WR018i005p01409.
Parker, G., and A. W. Peterson (1980), Bar resistance of gravel-bed streams, *J. Hydraul. Div. Am. Soc. Civ. Eng.*, *106*(10), 1559–1575.
Parker, G., P. C. Klingeman, and D. G. Mclean (1982), Bedload and size distribution in paved gravel-bed streams, *J. Hydraul. Div. Am. Soc. Civ. Eng.*, *108*(4), 544–571.
Powell, D. M., I. Reid, and J. B. Laronne (2001), Evolution of bed load grain size distribution with increasing flow strength and the effect of flow duration on the caliber of bed load sediment yield in ephemeral gravel bed rivers, *Water Resour. Res.*, *37*(5), 1463–1474, doi:10.1029/2000WR900342.
Prancevic, J. P., and M. P. Lamb (2015a), Unraveling bed slope from relative roughness in initial sediment motion, *J. Geophys. Res. Earth Surf.*, *120*, 479–489, doi:10.1002/2014JF003323.
Prancevic, J. P., and M. P. Lamb (2015b), Particle friction angles in steep mountain channels, *J. Geophys. Res. Earth Surf.*, *120*, 242–259, doi:10.1002/2014JF003286.
Prancevic, J. P., M. P. Lamb, and B. M. Fuller (2014), Incipient sediment motion across the river to debris-flow transition, *Geology*, *42*, 191–194, doi:10.1130/G34927.1.
Proffitt, G. T., and A. J. Sutherland (1983), Transport of non-uniform sediments, *J. Hydraul. Res.*, *21*(1), 33–43, doi:10.1080/00221688309499448.
Recking, A. (2009), Theoretical development on the effects of changing flow hydraulics on incipient bed load motion, *Water Resour. Res.*, *45*, W04401, doi:10.1029/2008WR006826.
Recking, A. (2010), A comparison between flume and field bed load transport data and consequences for surface-based bed load transport prediction, *Water Resour. Res.*, *46*, W03518, doi:10.1029/2009WR008007.
Recking, A. (2012), Influence of sediment supply on mountain streams bedload transport, *Geomorphology*, *175–176*, 139–150.
Recking, A., F. Liébault, C. Peteuil, and T. Jolimet (2012), Testing several bed load transport equations with consideration of time scales, *Earth Surf. Processes Landforms*, *37*, 774–789, doi:10.102/esp.3213.
Rickenmann, D. (1991), Hyperconcentrated flow and sediment transport at steep slopes, *J. Hydraul. Eng.*, *117*(11), 1419–1439, doi:10.1061/(ASCE)0733-9429(1991)117:11(1419).
Rickenmann, D. (2001), Comparison of bed load transport in torrents and gravel bed streams, *Water Resour. Res.*, *37*(12), 3295–3305, doi:10.1029/2001WR000319.
Rickenmann, D. (2012), Alluvial steep channels: Flow resistance, bedload transport prediction, and transition to debris flows, in *Gravel-Bed Rivers: Processes, Tools, Environments*, edited by M. Church, P. M. Biron, and A. G. Roy, John Wiley, Chichester, U. K., doi:10.1002/9781119952497.ch28.
Rickenmann, D., and A. Recking (2011), Evaluation of flow resistance in gravel-bed rivers through a large field data set, *Water Resour. Res.*, *47*, W07538, doi:10.1029/2010WR009793.
Rickenmann, D., M. Chiari, and K. Friedl (2006), SETRAC–A sediment routing model for steep torrent channels, in *River Flow 2006*, edited by E. C. T. L. Alves et al., Taylor and Francis, London, U. K., doi:10.1201/9781439833865.ch88.
Rickenmann, D., J. M. Turowski, B. Fritschi, A. Klaiber, and A. Ludwig (2012), Bedload transport measurements at the Erlenbach stream with geophones and automated basket samplers, *Earth Surf. Processes Landforms*, *37*(9), 1000–1011, doi:10.1002/esp.3225.
Schmid, B. (2011), Geschiebetransportuntersuchungen in einem Gebirgsbach, MS thesis, Versuchsanst. für Wasserbau, ETH Zurich, Zurich, Switzerland.
Shields, A. (1936), *Anwendung der Ähnlichkeitsmechanik und der Turbulenzforschung auf die Geschiebebewegung*, vol. 26, 26 pp., Eigenverl. der Preußischen Versuchsanst. für Wasserbau und Schiffbau Berlin, Berlin.
Shvidchenko, A. B., G. Pender, and T. B. Hoey (2001), Critical shear stress for incipient motion of sand/gravel streambeds, *Water Resour. Res.*, *37*(8), 2273–2283, doi:10.1029/2000WR000036.
Whiting, P. J., J. F. Stamm, D. B. Moog, and R. L. Orndorff (1999), Sediment-transporting flows in headwater streams, *Geol. Soc. Am. Bull.*, *111*(3), 450–466, doi:10.1130/0016–7606(1999)111<0450:STFIHS>2.3.CO;2.
Whittaker, J. G., W. E. Hickman, and R. N. Croad (1990), Riverbed stabilisation with placed blocks [online], in *IPENZ Annual Conference 1990, Proceedings of Engineering, Past, Present and Future: Building the Environment*, vol. 1, *Civil, Papers Prepared for the Conference, Wellington, February 12-17*, pp. 495–512, Inst. of Prof. Eng. N. Z., Wellington.

Wiberg, P. L., and J. D. Smith (1987), Calculations of the critical shear stress for motion of uniform and heterogeneous sediments, *Water Resour. Res.*, *23*(8), 1471–1480, doi:10.1029/WR023i008p01471.
Wilcock, P., J. Pitlick, and Y. Cui (2009), Sediment transport primer: Estimating bed-material transport in gravel-bed rivers, *Gen. Tech. Rep. RMRS-GTR-226*, U.S. Dep. of Agric., For. Serv., Rocky Mt. Res. Stn., Fort Collins, Colo.
Wilcock, P. R. (1988), Methods for estimating the critical shear stress of individual fractions in mixed-size sediment, *Water Resour. Res.*, *24*(7), 1127–1135, doi:10.1029/WR024i007p01127.
Wilcock, P. R. (2001), Toward a practical method for estimating sediment-transport rates in gravel-bed rivers, *Earth Surf. Processes Landforms*, *26*(13), 1395–1408, doi:10.1002/esp.301.
Wilcock, P. R., and J. C. Crowe (2003), Surface-based transport model for mixed-size sediment, *J. Hydraul. Eng.*, *129*(2), 120–128, doi:10.1061/(ASCE)0733-9429(2003)129:2(120).
Wilcock, P. R., S. T. Kenworthy, and J. C. Crowe (2001), Experimental study of the transport of mixed sand and gravel, *Water Resour. Res.*, *37*(12), 3349–3358, doi:10.1029/2001WR000683.
Williams, G. P., and D. L. Rosgen (1989), Measured total sediment loads (suspended and bedload) for 93 United States streams, *Open File Rep*. 89-67, U.S. Geol. Surv., Denver, Colo. [Available at http://pubs.usgs.gov/of/1989/0067/report.pdf.]
Wilson, K. (1987), Analysis of bed-load motion at high shear stress, *J. Hydraul. Eng.*, *113*(1), 97–103, doi:10.1061/(ASCE)0733–9429(1987)113:1(97).
Wohl, E. E. (2000), *Mountain Rivers*, AGU, Washington, D. C.
Wolman, M. G. (1954), A method of sampling coarse river-bed material, *Trans. AGU*, *35*(6), 951–956, doi:10.1029/TR035i006p00951.
Wong, M., and G. Parker (2006), Reanalysis and correction of bed-load relation of Meyer-Peter and Mueller using their own database, *J. Hydraul. Eng.*, *132*(11), 1159–1168, doi:10.1061/(ASCE)0733-9429(2006)132:11(1159).
Yager, E. M., J. W. Kirchner, and W. E. Dietrich (2007), Calculating bed load transport in steep boulder bed channels, *Water Resour. Res.*, *43*, W07418, doi:10.1029/2006WR005432.
Yager, E. M., W. E. Dietrich, J. W. Kirchner, and B. W. McArdell (2012a), Prediction of sediment transport in step-pool channels, *Water Resour. Res.*, *48*, W01541, doi:10.1029/2011WR010829.
Yager, E. M., J. M. Turowski, D. Rickenman, and B. W. McArdell (2012b), Sediment supply, grain protrusion, and bedload transport in mountain streams, *Geophys. Res. Lett.*, *39*, L10402, doi:10.1029/2012GL051654.